

Age-Related and Cuprizone-Induced Changes in Myelin and Transcription Factor Gene Expression and in Oligodendrocyte Cell Densities in the Rostral Corpus Callosum of Mice

J. Ronald Doucette · Rubin Jiao · Adil J. Nazarali

Received: 2 November 2009 / Accepted: 11 December 2009 / Published online: 9 January 2010
© Springer Science+Business Media, LLC 2010

Abstract During aging, there is a decrease both in the stability of central nervous system (CNS) myelin once formed and in the efficiency of its repair by oligodendrocytes (OLs). To study CNS remyelination during aging, we used the cuprizone (a copper chelator) mouse model. Inclusion of cuprizone in the diet kills mature OLs and demyelinate axons in the rostral corpus callosum (CC) of mice, which enabled us to characterize age-related changes (i.e., 2–16 months of age) in glial cell response during the recruitment (i.e., demyelination) and differentiation (i.e., remyelination) phases of myelin repair. We have found that the time between 12 and 16 months of age is a critical period during which there is an age-related decrease in the number of OL lineage cells (Olig2^{Nuc}+ve/GFAP–ve cells) in the rostral CC of both control mice and mice recovering from cuprizone-induced demyelination. Our results also show there was an age-related impaired recruitment of progenitor cells to replace lost OLs in spite of there being no major age-related decrease in the size of the progenitor cell pool (PDGF α R+ve/GFAP–ve, and Olig2^{Nuc}+ve/PDGF α R+ve cells). However, there were cuprizone-induced increased numbers of astrocyte progenitor cells (Olig2^{Cyto}+ve/PDGF α R+ve) in these same mice; thus

PDGF α R+ve progenitor cells in mice as old as 16 months of age retain the ability to differentiate into astrocytes, with this fate choice occurring following cytoplasmic translocation of Olig2. These data reveal for the first time age-related differences in the differentiation of PDGF α R+ve progenitor cells into OLs and astrocytes and lead us to suggest that during aging there must be a transcriptional switch mechanism in the progenitor cell fate choice in favor of astrocytes. This may at least partially explain the age-related decrease in efficiency of OL myelination and remyelination.

Keywords Aging · Astrocytes · Myelin · Oligodendrocytes · Olig2 · Nkx2.2 · PDGF α R · MOG · MBP

Introduction

Myelin is the fatty substance forming the core component of the sheath surrounding axons of the central nervous system (CNS) (see Table 1 for list of abbreviations). In the CNS, this myelin sheath is made by OLs (Collarini et al. 1991; Zeller et al. 1985), and therefore the myelinating ability of these cells is critical to the proper repair of CNS injury. In the human brain, OL progenitor cells continue to be recruited to myelinate axons de novo in white matter of prefrontal, parietal, and temporal areas well into the fifth decade of life as part of the normal age-related time schedule of CNS myelination (Bartzokis 2004a, b; Bartzokis et al. 2004a). As an animal ages, each newly formed OL myelinates increasing numbers of axonal segments, thus inflicting high metabolic demands on these OLs and making them especially susceptible to a variety of insults. These insults can include any injury to the brain,

J. Ronald Doucette
Department of Anatomy and Cell Biology, College of Medicine,
University of Saskatchewan, Saskatoon, SK S7N 5E5, Canada

J. Ronald Doucette · A. J. Nazarali
Cameco MS Neuroscience Research Center, City Hospital,
Saskatoon, SK S7K 0M7, Canada

R. Jiao · A. J. Nazarali (✉)
Laboratory of Molecular Biology, College of Pharmacy and
Nutrition, 116 Thorvaldson Building, 110 Science Place,
University of Saskatchewan, Saskatoon, SK S7N 5C9, Canada
e-mail: aj.nazarali@usask.ca

Table 1 List of abbreviations

ANOVA	Analysis of variance
APC	Anti-adenomatous polyposis coli
CC	Corpus callosum
cDNA	Complementary DNA
CGT	Ceramide galactosyltransferase
CNS	Central nervous system
CNTF	Ciliary neurotrophic factor
DNA	Deoxyribonucleic acid
Cre	Cre recombinase
ER	Estrogen receptor
FGF	Fibroblast growth factor
GFAP	Gliial fibrillary acidic protein
GFP	Green fluorescent protein
MBP	Myelin basic protein
MOG	Myelin oligodendrocyte glycoprotein
NG2	Chondroitin sulfate proteoglycan
Ngn3	Neurogenin 3
Nkx2.1/ Nkx2.2	NK2 transcription factor related, locus 1 or 2
Nkx6.1/ Nkx6.2	NK6 transcription factor related, locus 1 or 2
OL(s)	Oligodendrocyte(s)
Olig	Oligodendrocyte transcription factor
Olig2 ^{Nuc} +ve	Olig 2, nuclear expression
Olig2 ^{Cyto} +ve	Olig 2, cytoplasmic expression
PBS	Phosphate buffered saline
PCR	Polymerase chain reaction
PDGF	Platelet-derived growth factor
PDGF α R	Platelet-derived growth factor alpha-receptor
pMN	Motor neuron progenitor
qRT-PCR	Quantitative real time RT-PCR
ROSA-EGFP	Enhanced green fluorescent protein gene in the ROSA locus
RNA	Ribonucleic acid
RT	Reverse transcriptase
RQ	Relative quantity
SM-PBST	3% skim milk and 1% Triton X-100 in 0.1 M PBS
SEM	Standard error of mean
Sox	SRY-box containing gene
STAT3	Signal transducer and activator of transcription 3
TF(s)	Transcription factor(s)
TGF β	Transforming growth factor beta
TrR	Treatment (cuprizone) recovery mice

including for example chemical exposure, stroke or accumulation of β -amyloid plaques in Alzheimer's disease.

Recovery from these insults and other types of injury is compromised by an age-related decline in OL remyelination efficiency (Ando et al. 2003; Chari et al. 2003; Franklin et al. 2002; Peters 2002b; Rist and Franklin 2008; Sandell and Peters 2002; Sim et al. 2002; Sloane et al.

2003). In non-human primates, myelin sheath abnormalities in cortical white matter correlate with age and diminished cognitive status (Peters 2002a, b; Peters and Sethares 2002). Demyelination that ensues in the white matter of association areas of the human brain in older individuals, and the progressively poorer repair of this pathophysiology as one gets older, disrupts neural impulse transmission and impairs higher cognitive functions, including memory (Bartzokis 2004a, b; Bartzokis et al. 2004a; Benes 2004; Braak and Del Tredici 2004; Connor 2004; Noble 2004).

The age-related decreased efficiency of OL myelination and remyelination is due to an impaired recruitment and differentiation of OL progenitor cells (Ando et al. 2003; Chari et al. 2003; Franklin et al. 2002; Peters 2002b; Rist and Franklin 2008; Sim et al. 2002). Changes in transcriptional control likely underlie the impaired recruitment of OL progenitor cells into demyelinated lesions and/or the differentiation of these cells into myelinating glia (Franklin et al. 2002; Rist and Franklin 2008; Shen et al. 2008; Sim et al. 2002). Transcription factors (TFs) coordinate the orderly changes of gene expression that occur during the recruitment and differentiation of these progenitors (Nicolay et al. 2007; Wegner 2000a, b, 2001). Very little is known with regard to how TFs coordinate gene expression in OL progenitor cells for remyelination of CNS axons in adult mammals, or for the de novo myelination that occurs in many areas of cortical white matter in humans even into the fifth decade of life (Bartzokis 2004a, b; Bartzokis et al. 2004a). The expression profiles of growth factors (i.e., PDGF, FGF, and TGF- β) known to be important for oligodendrogenesis are temporally delayed in older animals compared to young adults and may contribute to a slower recruitment and differentiation of OL progenitor cells (Franklin et al. 2002; Hinks and Franklin 2000; Rist and Franklin 2008). Platelet-derived growth factor alpha-receptor (PDGF α R) is a marker of early OL progenitors. In the embryonic spinal cord, PDGF α R+ve OL progenitor cells initially arise from a distinct region of the ventral ventricular zone and exhibit unique expression domains in the embryonic brain, which is suggestive of distinct OL progenitor lineages (Nicolay et al. 2007).

The lamellipodial expansion of the cytoplasmic processes of pre-myelinating OLs along and around axons is a dynamic event orchestrated by OL-axon interactions that ultimately lead to the formation of a compact myelin sheath (Knobler et al. 1974). However, the transcriptional control and the signaling pathways that collectively regulate and govern CNS myelinogenesis in vivo are not well defined. As discussed in our recent review (Nicolay et al. 2007), various TFs including Olig1, Olig2, Nkx6.2, and Sox10 favor OL maturation. We described transcriptional control of oligodendrogenesis by examining TFs not in isolation but in the context of a transcriptional network.

Although one can make fairly confident statements about roles of some individual TFs in OL myelin gene expression and myelination, functional linkages between TFs and/or signaling pathways require more conjecture. Virtually nothing is known with regard to changes in TF expression that may contribute to the age-related decline in remyelination efficiency by OLs. Even with respect to embryonic development, information regarding the TF regulation of oligodendrogenesis following specification is lacking (Nicolay et al. 2007). Notable exceptions exist for plausible roles of a handful of TFs, with the likely roles of some of these TFs reviewed in Nicolay et al. (2007).

Several animal models have been used to study morphological, cellular, and molecular mechanisms regulating CNS myelin repair in young animals (Hall 1972; Herndon et al. 1977; Lang et al. 1984; Lyman et al. 1985; Yajima and Suzuki 1979). Each model mimics some, but not all, of the pathological and neurological sequelae of MS, the main demyelinating disease in humans. In the present study we used the cuprizone model to investigate changes in TFs (*Olig2* and *Nkx2.2*) and in myelinating gene (*MOG*, *CGT*) expression during OL myelination/remyelination because the demyelination is easily inducible, localized, and predictable, and the model provides excellent anatomical reproducibility of the lesions (Arnett et al. 2004; Hiremath et al. 1998). This neurotoxicant typically is used in mice at 8–10 weeks of age (Carey and Freeman 1983; Jurevics et al. 2002; Mason et al. 2003; Morell et al. 1998; Stidworthy et al. 2003) and has not been used in mice past 10 months of age (Shen et al. 2008). We show in this study it can be used to study age-related changes in the OL expression of TFs and myelin genes during remyelination up to at least 16 months of age. As a copper chelator, cuprizone reproducibly demyelinates select fiber tracts in the mouse brain (Matsushima and Morell 2001); tracts susceptible to this demyelination are the CC, in particular the most rostral part (Carey and Freeman 1983; Jurevics et al. 2002; Mason et al. 2003; Morell et al. 1998; Stidworthy et al. 2003), and the superior cerebellar peduncle (Komoly et al. 1992; Ludwin 1978, 1979, 1980; Ludwin and Sternberger 1984; Stidworthy et al. 2003). When cuprizone is withdrawn from the diet, remyelination takes place spontaneously. More importantly, we show in the present study that the cuprizone model is appropriate for use in mice as old as 16 months of age, thus enabling us to follow age-related changes in the expression profile of several OL genes during the cuprizone-induced demyelination (OL progenitor recruitment) and subsequent remyelination (OL differentiation) phases in the rostral CC. The cuprizone model can tease out age-related changes in transcriptional regulation most directly related to OL remyelination, as cuprizone neither generates a lymphocytic response (Armstrong et al. 2002) nor breaks down the blood–brain barrier (Bakker and Ludwin 1987; Kondo et al. 1987).

Methods

Animals Used in the Project

Tissues from a total of 72 C57BL/6 mice were used to collect the data reported in this study. They were purchased from Jackson Laboratories, Bar Harbor, Maine. The study design (see Fig. 1) and the protocol for the daily care of the mice were approved by the Animal Protocol Review Committee (University of Saskatchewan); food and water were available to all mice ad libitum. This aging study used mice varying in age from 2 to 16 months old. We estimate the comparable ages in human years to be <20 years (2 month-old mice), ~30 years (6 month-old mice), ~42 years (12 month-old mice), and ~50 years (16 month-old mice) of age (Life Phase Equivalencies were determined from The Jackson Laboratory research webpage of Dr. David E. Harrison <http://research.jax.org/faculty/harrison/gerl/LifeSpan1.html#VD>). We purchased the mice at 2, 6, and 8 months of age; the 8 month-old mice were aged to 12 and 16 months of age in the University of Saskatchewan's animal facility. We used 18 mice for each of the four age groups.

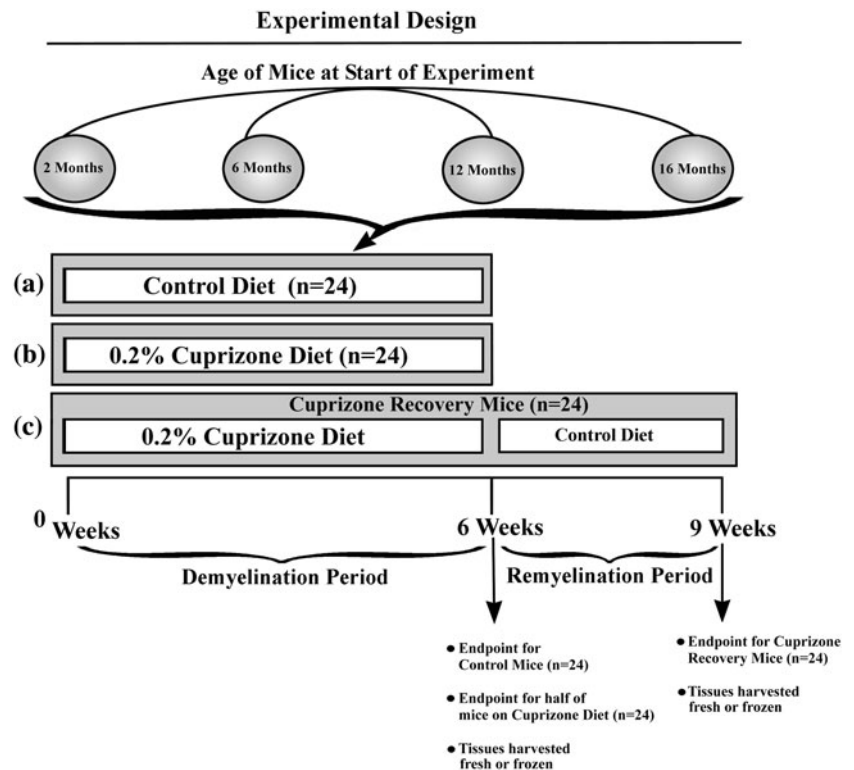
Cuprizone-Induced Demyelination

Cuprizone (0.2% by weight, mixed in with milled chow) was fed to young adult (2 and 6 months old) and aged (12 and 16 months old) C57BL/6 mice for a period of 6 weeks (Armstrong et al. 2002); control wild-type mice were fed normal milled chow. The body weight of each mouse was measured on a daily basis. At the end of the sixth week, all of the control mice and half of the mice on the cuprizone diet were euthanized. The remaining mice were switched to a diet of normal milled chow for 3 weeks prior to the animals being euthanized. With this experimental design (Fig. 1), there were three treatment groups: (a) control mice, which were fed normal milled chow for 6 weeks; (b) cuprizone mice, which were fed a cuprizone-containing diet for 6 weeks; and (c) cuprizone recovery mice, which were fed cuprizone for the first 6 weeks followed by normal milled chow for the next 3 weeks. Six mice were used for each of the three treatments at each of the four ages. Half of the mice for each treatment and age were used for immunofluorescent microscopy and the remaining half for collecting tissue for quantitative RT–PCR (qRT–PCR).

Necropsy and Tissue Dissection

The mice ($n = 36$) designated for the immunofluorescence quantification of OLs and myelin protein immunostaining in the rostral CC were cardiac-perfused (Blakemore and Crang 1988; Blakemore et al. 1990; Boyd et al. 2004), first

Fig. 1 A diagram illustrating experimental design of the study. There were three treatment groups: **a** control mice, which were fed normal milled chow for 6 weeks; **b** cuprizone mice, which were fed a 0.2% cuprizone-containing diet for 6 weeks; and **c** cuprizone recovery mice, which were fed 0.2% cuprizone diet for the first 6 weeks followed by normal milled chow for the next 3 weeks. Six mice were used for each of the three treatments at each of the four ages. Half of the mice for each treatment and age were used for immunofluorescent microscopy and the remaining half for collecting tissue for quantitative RT-PCR (qRT-PCR)



with PBS and then with fresh cold 4% paraformaldehyde in PBS (pH 7.4). The brains were dissected from the skull and fixed overnight in 4% paraformaldehyde in PBS at 4°C. The next day the brains were rinsed in ice-cold 30% sucrose in PBS and stored in fresh 30% sucrose in PBS for 2–3 days prior to cryostat sectioning. Each mouse brain was separated down the midline. One half of each brain was used for cutting cryostat coronal sections (8 μ m thick) through the frontal lobe and rostral part of the CC (Fig. 2). The other half of each brain was used to obtain cryostat sagittal sections (8 μ m thick) for immunostaining with antibodies to myelin basic protein (MBP) and myelin oligodendrocyte glycoprotein (MOG) to provide a subjective assessment of the demyelination and remyelination in the rostral CC (Fig. 4 and 5). Mice ($n = 36$) providing rostral CC tissue for qRT-PCR analysis were euthanized using carbon dioxide inhalation, after which the brains were frozen in liquid nitrogen. These brains were stored at -80°C until all 36 mice had been euthanized and their brain tissue collected and frozen.

Quantitative Real Time-PCR

Total RNA was isolated from excised rostral CC (Fig. 2) from brains of control (normal mouse chow), cuprizone and cuprizone recovery mice (2–16 months old) using the RNeasy® Protect Mini Kit (Qiagen) as per the manufacturer's protocol. RNA concentration was determined by

optical density. First-strand DNA synthesis was performed using the SuperScript first-strand synthesis system for RT-PCR (Invitrogen) and random decamer primers, as per the manufacturer's protocol. The final concentration of RNA for all RT reactions was 20 ng/ μ L.

Gene expression was quantified using the Taqman primers and labeled probe system and the ABI 7300 (Applied Biosystems). cDNA samples from the rostral CC of control, cuprizone and cuprizone recovery mice were tested for *PDGF α R*, *Olig2*, *MOG*, ceramide galactosyltransferase (*CGT*) and *Nkx2.2*. All reactions were performed using the Taqman Universal Master Mix (2X), FAM-labeled Taqman Gene Expression assays for gene of interest, VIC-labeled Taqman endogenous control β -actin, and 10 ng of cDNA. All reactions were run in replicates of four, with cDNA samples from three mice per experimental group being used for each reaction. Thermocycling parameters were as follows: 2 min at 50°C, 10 min at 95°C, 40 cycles of 15 s at 95°C plus 70 s at 60°C.

Immunostaining of Tissue Sections for Cell Counting

The brains were embedded in optimal cutting temperature compound (Tissue-Tek), serially sectioned (8 μ m) in either the coronal or sagittal planes with a cryostat, and collected onto gelatin-coated coverslips. The sections were air dried at room temperature for 30 min. The sections were then rehydrated in 0.1 M PBS twice (10 min each), after which

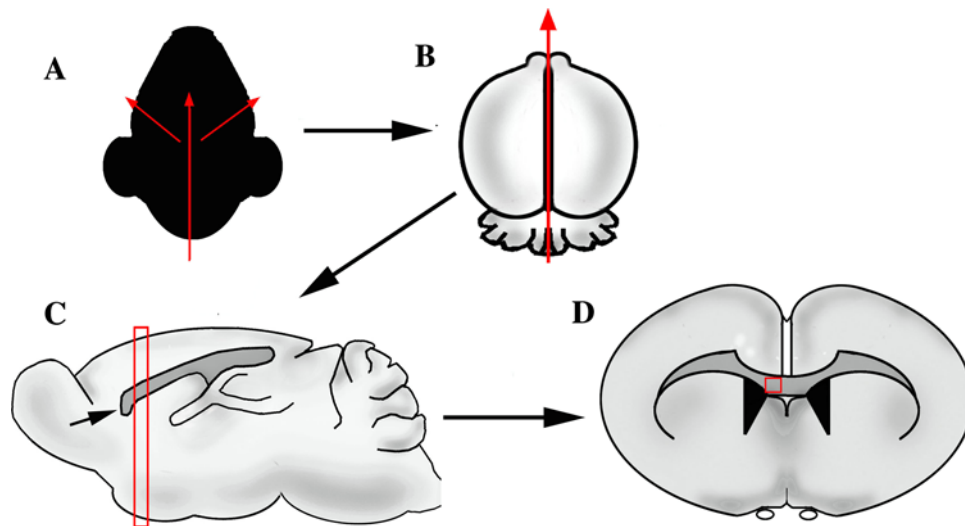


Fig. 2 A diagram summarizing how the brain was dissected for cutting sagittal and coronal cryostat sections. **a** The brain is removed from the skull and separated down the midline, **b** thus dividing the brain into a right and a left half. **c** A midsagittal section of the right cerebral hemisphere, including the genu (arrow) and body of the CC. Myelin protein immunostaining was done on cryostat sagittal tissue sections to see age-related differences in cuprizone-induced demyelination in the CC and the extent of myelin repair in the cuprizone recovery mice. The long, thin rectangle passes through the rostral part

of the body of the CC and indicates the plane of section for the drawing in **d**, which shows the coronal plane through the brain. This coronal plane was used for all of the immunostaining for quantifying cell densities, with the quantification done on digital images captured from the medial part of the CC, which is indicated by the boxed area in **d**. The CC tissue used for qRT-PCR was obtained from a comparable area within the medial aspect of this myelinated fiber tract

they were blocked in 3% SM-PBST (3% skim milk and 1% Triton X-100 in 0.1 M PBS) for 40 min. Sections were then exposed to the primary antibodies in 0.1 M PBS at 4°C overnight (Hao et al. 1999). Except for tissue sections immunostained with antibodies to MBP or MOG, all sections were double-labeled with two antibodies. The mouse anti-MBP (Sternberger Monoclonals) was used at a dilution of 1:1,000 and the mouse anti-MOG (gift from Dr. M. Gardinier) was used at a dilution of 1:3. Double-labeling of tissue sections to be used for quantitation of the glial cell response to aging and to cuprizone-induced demyelination included these combinations: mouse anti-glial fibrillary acidic protein (GFAP; 1:1,000; Sigma)/rabbit anti-Olig2 (1:1,000; gift from Dr. H. Takebayashi), rabbit anti-Olig2/rat anti-PDGFR (1:100; BD Pharmingen), rabbit anti-GFAP (1:1,000; Dimension Labs)/rat anti-PDGFR.

The following morning, the tissue sections were rinsed twice in 0.1 M PBS. The secondary antibodies were then applied for 45 min at room temperature. The secondary antibody (Invitrogen) combinations used included: to detect GFAP/Olig2 double immunostaining we used Alexa Fluor 488 conjugated goat anti-mouse IgG (1:200)/Alexa Fluor 594 conjugated goat anti-rabbit IgG (1:400); for Olig2/PDGFR we used Alexa Fluor 488 conjugated goat anti-rabbit IgG (1:200)/Alexa Fluor 594 conjugated goat anti-rat IgG (1:400); for GFAP/PDGFR we used Alexa Fluor 488 conjugated goat anti-rabbit IgG (1:200)/Alexa

Fluor 594 conjugated goat anti-rat IgG (1:400); for both MBP and MOG single immunostaining we used Alexa Fluor 594 conjugated goat anti-mouse IgG (1:400). After two washes in 0.1 M PBS, the sections were counterstained with Hoechst 33258 (2 µg/ml) to visualize the nuclei. Finally, the sections were rinsed twice in 0.1 M PBS, mounted in Prolong (Molecular Probes) anti-quenching mounting medium, and then examined with fluorescence microscopy.

Blinded Cell Counts

Upon completion of the immunofluorescent staining, each tissue section was assigned an alphanumeric code and all cell counts were done blindly. Three digital images were taken of each coded double immunostained tissue section; the images were captured from three separate fields within the medial aspect of the rostral CC (using a 20× objective). The data collected from each image captured from a double immunostained tissue section were the density of cells (i.e., number of cells per 500 µm²) that co-expressed two proteins (e.g., Olig2^{Nuc}+ve/PDGFR+ve) or expressed only one of the proteins (e.g., Olig2^{Nuc}+ve/GFAP−ve). The total number of Hoechst+ve nuclei was also determined for each image. These cell counts were done using the software program Image Pro® Plus 6.2 (Olympus Canada Inc., Markham, ON).

Statistical Analyses

All quantitative data were statistically compared using a two-way analysis of variance (ANOVA) (Prism® Software Corporation). The significance levels for main effects and for an interaction effect are found in Table 2 for each set of data depicted in the histograms (Figs. 3, 6, 7, 8, 10, and 11). Multiple post hoc comparisons were performed with Bonferroni's multiple comparison post-test (Prism software program). The significance level for both the ANOVA and the post-test was set at $P < 0.05$.

Results

Health Condition of 2- to 16-Month Old Mice Fed the Control or Cuprizone Diet

Each mouse used in this study was weighed prior to initiating the study (i.e., day zero) as well as on a daily basis until they were killed for immunostaining or for qRT-PCR analysis. All mice were also observed daily for changes in behavior. This daily weighing and checking of each mouse enabled us to monitor the effect of the cuprizone-containing diet on their mobility and eating habits, as well as on their health status (e.g., condition of fur and body weight). Other than weight loss, and a few mortalities or dermatitis problems, practically all of the mice remained in good health until they were killed for immunostaining or qRT-PCR. At the beginning of the study, the Director of the Health Sciences Animal Facility was asked to examine some of the cuprizone-fed mice and it was her opinion that in spite of the weight loss the mice were healthy enough to continue the study. Two mice (16 months of age) being fed the cuprizone diet developed skin lesions unrelated to the cuprizone diet; the mice with dermatitis, on the advice of the Assistant Director of the Animal Care Unit, were euthanized prior to completion of the 6 weeks of cuprizone feeding and were replaced with alternate 16 month-old mice. An additional two mice (12 months of age) died during the cuprizone feeding and they were replaced with other mice of that same age that were fed the cuprizone diet for 6 weeks.

As indicated in Table 2, the two-way ANOVA on the day zero body weights for the controls, cuprizone and cuprizone recovery mice at each of the four ages showed only a significant main effect of age, which was not unexpected since there was a 14-month difference in age between the youngest and oldest mice (Fig. 3a). Most importantly, however, the absence of a significant treatment effect ($P > 0.05$) indicates that at each age the mice in the different treatment groups had similar body weights at the beginning of the experiment. Bonferroni's post-test was

used to assess the statistical significance of age-related differences in body weight within each group of mice. Between 2 and 16 months of age, there was a 1.75-fold (control mice), 1.72-fold (cuprizone mice), and 1.82-fold (cuprizone recovery mice) increase in body weight during the intervening 14 months (Fig. 3a).

The body weights that were measured on each day of the 6 week period over which the mice were fed either the control diet or the cuprizone-containing diet were expressed as a percentage of the day zero body weight for that mouse. The percentage of day zero body weight was averaged for each 7 day period to provide an average percentage body weight for Week 1, Week 2, etc. The average percentages of day zero body weight for the 3 (Fig. 3b) and 6 (Fig. 3c) week time periods were analyzed separately using a two-factor ANOVA (see Table 2), with treatment (i.e., control, and cuprizone mice) and age (i.e., 2, 6, 12, and 16 months of age) being the two independent variables. Not surprisingly, mice on the cuprizone diet lost weight, with the size of the weight loss being influenced both by the age of the mouse and by how many weeks they had been on the cuprizone diet. In general, 6 month-old cuprizone mice lost the most weight while on the cuprizone diet, with these mice having lost, respectively, 15.4% by Week 3 and 16.2% by Week 6 (Fig. 3b, c). Over the same 6 week time period, the 2 month-old cuprizone mice lost the least amount of weight, with the weight loss at Week 6 averaging 5.0% (Fig. 3c).

For the cuprizone recovery mice, the average percentage of day zero body weights at the 9 week time point indicate the extent to which 3 weeks on control diet enabled the mice to recover from the weight loss they experienced during the preceding 6 weeks on the cuprizone-containing diet (Fig. 3d). A two-factor ANOVA was used to compare the Week 6 and Week 9 (i.e., survival times) average percentage of day zero body weights at each of the four ages (see Table 2). The presence of significant main effects of survival time and age, but the lack of an interaction effect is because the Week 9 average percentage of day zero body weights were consistently higher at all ages than those for Week 6. Bonferroni's post-test showed the higher Week 9 average percentage of day zero body weights compared to the Week 6 values reached statistical significance for both the 2 (18.1% higher) and 6 (16.8% higher) month-old cuprizone recovery mice ($P < 0.05$). Bonferroni's post-test also revealed that the weight gain detected by Week 9 (i.e., after a 3 week period on control diet) was significantly larger for 2 (18.1%) month-old cuprizone recovery mice than for either the 12 (10.5%) or 16 (6.5%) month-old cuprizone recovery mice ($P < 0.05$). Thus, the oldest mice did not recover as well, in terms of body weight gain, as did the younger mice (Fig. 3d).

Table 2 Statistical summaries

		Two-way ANOVA effects (statistical significance)			
Fig. 3	3A	– Age ($P < 0.0001$)	3B	– Age ($P = 0.0008$)	
		– Treatment ($P > 0.05$)		– Treatment ($P < 0.0001$)	
		– Interaction ($P > 0.05$)		– Interaction ($P > 0.05$)	
	3C	– Age ($P < 0.0001$)	3D	– Age ($P < 0.0004$)	
		– Treatment ($P < 0.0001$)		– Treatment ($P < 0.0001$)	
		– Interaction ($p = 0.02$)		– Interaction ($P > 0.05$)	
Fig. 6	6A	– Age ($P < 0.0001$)	6B	– Age ($p = 0.04$)	
		– Treatment ($P < 0.0001$)		– Treatment ($P > 0.05$)	
		– Interaction ($P < 0.0001$)		– Interaction ($P < 0.0001$)	
Fig. 7	7A	– Age ($P < 0.0001$)		–	
		– Treatment ($P < 0.0001$)			
		– Interaction ($P < 0.0001$)			
Fig. 8	8A	– Age ($P = 0.0001$)	8B	– Age ($P = 0.0001$)	
		– Treatment ($P > 0.05$)		– Treatment ($P < 0.009$)	
		– Interaction ($P < 0.0001$)		– Interaction ($P < 0.0001$)	
	8C	– Age ($P < 0.0001$)		–	
		– Treatment ($P > 0.05$)			
		– Interaction ($P = 0.04$)			
Fig. 10	10A	– Phenotype ($P > 0.0001$)	10B	– Phenotype ($P > 0.0001$)	
		– Treatment ($P > 0.05$)		– Treatment ($P > 0.05$)	
		– Interaction ($P < 0.0001$)		– Interaction ($P = 0.02$)	
	10C	– Phenotype ($P > 0.0001$)	10D	– Phenotype ($P > 0.0001$)	
		– Treatment ($P < 0.0001$)		– Treatment ($P > 0.05$)	
		– Interaction ($P < 0.0001$)		– Interaction ($P = 0.004$)	
Fig. 11	11A	– Phenotype ($P > 0.05$)	11B	– Phenotype ($P < 0.001$)	
		– Treatment ($P < 0.0001$)		– Treatment ($P < 0.0001$)	
		– Interaction ($p = 0.009$)		– Interaction ($P > 0.05$)	
	11C	– Phenotype ($P > 0.05$)	11D	– Phenotype ($P < 0.0001$)	
		– Treatment ($P < 0.0001$)		– Treatment ($P > 0.05$)	
		– Interaction ($P = 0.0003$)		– Interaction ($P = 0.003$)	

Effectiveness of Cuprizone Model to Induce Demyelination of Rostral CC in Mice up to 16 Months of Age

First, it should be noted that there did not appear to be any obvious age-related loss of MBP (Fig. 4) or MOG (Fig. 5) immunostaining in the rostral CC of mice fed a control diet. To assess the effectiveness of the 0.2% cuprizone diet in demyelinating the rostral CC of mice aged 2–16 months, select coronal and sagittal tissue sections from control and cuprizone-fed mice were immunostained with antibodies to MBP or MOG. Using fluorescence optics, a subjective examination of the immunostained sections in all three mice for each group showed a similar pattern of demyelination in the rostral CC across all the ages (Figs. 4 and 5).

Rarely was the entire thickness of the rostral CC demyelinated, with usually a rim of MBP and MOG

immunostaining being retained where the white matter abutted the gray matter. The demyelination was also primarily limited to the body of the CC (Fig. 5). These data indicate a similar loss of MBP and MOG immunostaining in the rostral CC of cuprizone-fed mice, regardless of age. Age-related differences were seen, however, in the cuprizone recovery mice, that is, in the rostral CC of mice fed control mouse chow for 3 weeks after having been fed a cuprizone-containing diet for 6 weeks. There was noticeably less immunostaining with either MBP or MOG in the rostral CC of 12- and 16 month-old cuprizone recovery mice compared to the 2- and 6 month-old cuprizone recovery mice. This subjective examination of the immunostained sections suggests there may be age-related differences in gene expression and OL cell densities in the rostral CC in response to cuprizone-induced demyelination.

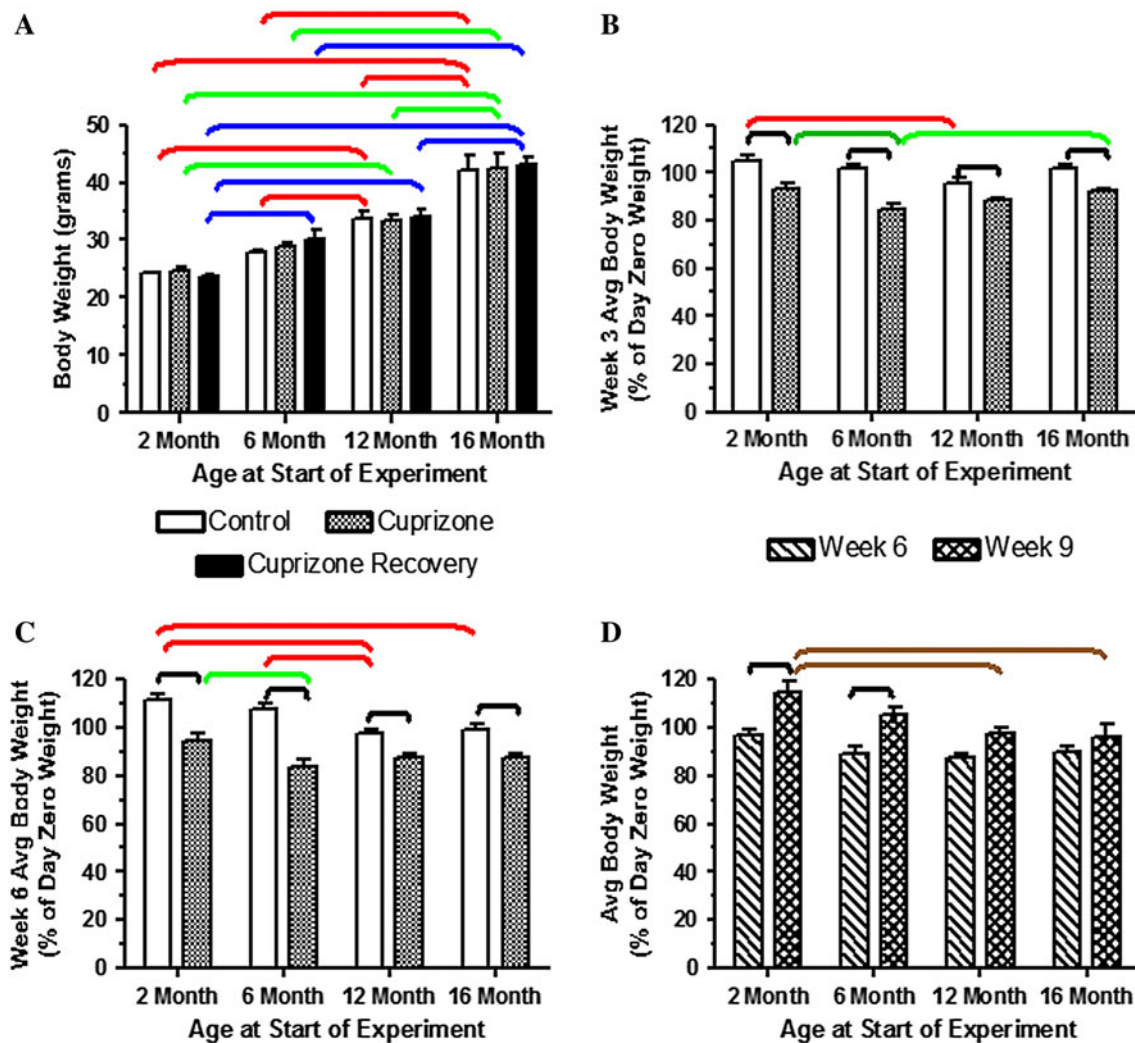


Fig. 3 Histograms depicting age-related and treatment-related changes in body weight. Three mice were used for each treatment and for each age. **a** The average day zero body weight (in grams) in 2–16 month-old controls, cuprizone and cuprizone recovery mice. **b** and **c** Week 3 and Week 6, respectively, average body weights of 2–16-month-old mice expressed as a percentage of day zero weight. **d** Week 6 and Week 9 average body weights of 2–16 month-old cuprizone recovery mice expressed as a percentage of day zero

weight. The brackets in color denote significant age-related differences within a group (*red* = control, *green* = cuprizone, *blue* = cuprizone recovery), whereas black brackets denote significant treatment-related differences and brown brackets denote significant difference between cuprizone recovery groups (Bonferroni's post-test; significance level of $P \leq 0.05$). For interpretation of the references to color in this figure legend, the reader is referred to the web version of the article

Changes in Myelin Gene Expression During Normal Aging

To determine if there were age-related changes in myelin gene expression, qRT-PCR was done to measure the expression levels of two myelin genes in the rostral CC of control mice. The two genes chosen for analysis are expressed at early (i.e., *CGT*) and late (i.e., *MOG*) stages of OL expression of a myelinating phenotype. The RQ values for each gene that were obtained by qRT-PCR for each mouse in each treatment group and at each age were normalized to the mean RQ value of the respective 2 month

control mice. Normalized RQ values greater than 1 indicate increased gene expression relative to the 2 month control levels, while values less than 1 signify decreased levels of gene expression relative to the 2 month control. The statistical significance of differences in normalized RQ values were assessed using a two-way ANOVA (Fig. 6 and Table 2).

The levels of *MOG* gene expression in control mice underwent a significant age-related decrease (Fig. 6a), with the normalized RQ values for *MOG* at 16 months of age (0.24 ± 0.01 ; SEM) being fourfold lower than that of the 2 month-old control mice ($P < 0.05$). There was also an

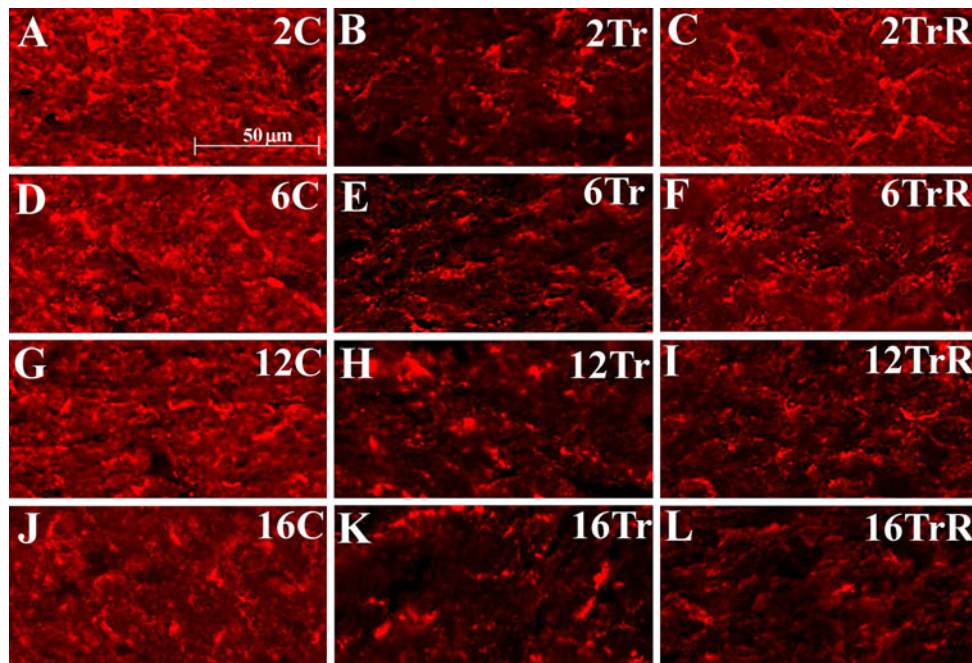


Fig. 4 Immunohistochemical analysis of myelin basic protein (MBP) in coronal sections through the rostral CC of 2, 6, 12, and 16 month-old mice, untreated control (**a, d, g, and j**), 6 week cuprizone treated (**b, e, h, and k**), and 6 week cuprizone treatment followed by 3 week recovery (**c, f, i, and l**). Cuprizone-fed mice show decreased expression of MBP in rostral CC (**b, e, h, k** compared to **a, d, g, j**)

age-related decreased expression of the *CGT* gene in control mice (Fig. 6b), with the normalized RQ value of 16-month-old mice (0.60 ± 0.02) being significantly lower than the expression levels seen in mice 2 months of age ($P < 0.05$). However, in contrast to the 4-fold reduction in *MOG* expression in the rostral CC of control mice, there was less than a 2-fold age-related reduction in *CGT* expression in the rostral CC of these same mice.

Changes in Myelin Gene Expression in Response to Cuprizone-Induced Demyelination

We predicted myelin gene expression in the CC would be decreased in response to cuprizone treatment since all myelinating OLs would be killed. For *MOG* gene expression, the expected cuprizone-induced reduction was seen only at 2 months of age (Fig. 6a), where the normalized RQ values in the rostral CC of cuprizone (0.33 ± 0.02) mice was significantly decreased compared to that of age-matched control mice ($P < 0.05$). However, in mice of 6, 12, and 16 months of age the levels of gene expression for *MOG* in the rostral CC of cuprizone mice were not significantly different from those of age-matched control mice ($P > 0.05$) (Fig. 6a). In contrast to normal aging (i.e., control mice), there were no age-related differences in *MOG* expression in the rostral CC of cuprizone mice

that recovers in 2 and 6 month-old mice (**c, f** compared to **a, d**) after a period of 3 weeks but only partially recovers in the 12 and 16 month-old mice (**i, l** compared to **g, j** and **c, f**). Thus, when the cuprizone model is used on mice of 2, 6, 12, and 16 months of age, the impaired efficiency of OL remyelination is first evident at 12 months of age. $n = 3$, bar = 50 μm

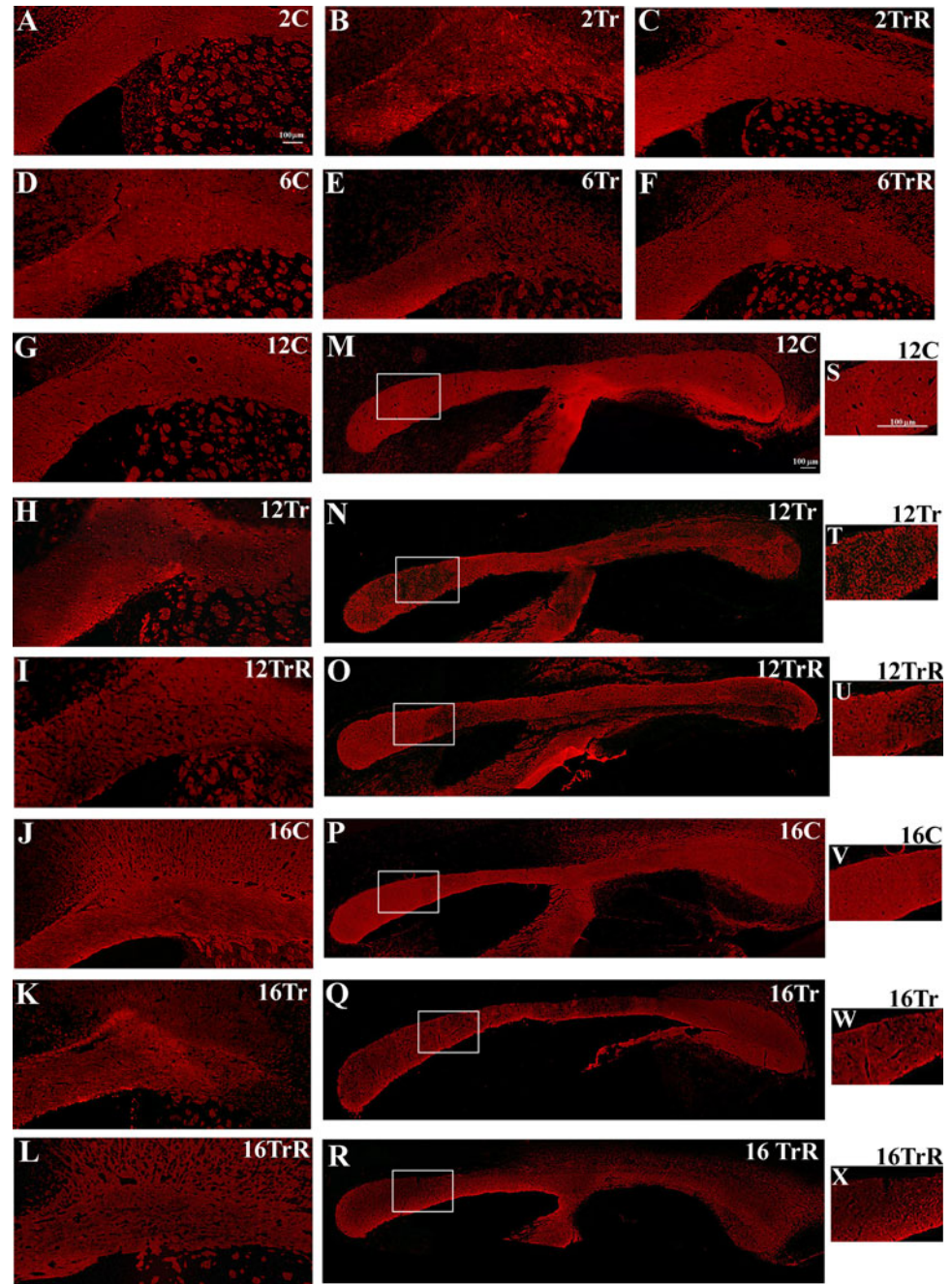
($P > 0.05$), thus showing that expression of the *MOG* gene in response to cuprizone-induced demyelination was similar at all four ages (Fig. 6a).

The significant interaction between age and treatment, as revealed by the two-way ANOVA on the *CGT* normalized RQ values, and the absence of a main effect of treatment means that the cuprizone treatment differentially affected *CGT* gene expression by cells of the rostral CC, dependent on the age of the mouse. The only statistically significant difference in the normalized RQ values that was revealed by Bonferroni's post-test was a significantly increased level of expression in 12 month-old cuprizone (1.02 ± 0.15) mice compared to that of age-matched (0.48 ± 0.06) control mice ($P < 0.05$) (Fig. 6b). This effect of cuprizone treatment on inducing *CGT* expression in 12 month-old mice was not simply a function of the cuprizone being fed to older mice since the *CGT* expression level in 16 month-old cuprizone (0.71 ± 0.06) mice was not significantly different from that of age-matched control mice (0.60 ± 0.02) ($P > 0.05$).

Changes in Myelin Gene Expression After 3 Weeks of Recovery from Cuprizone-Induced Demyelination

The *MOG* and *CGT* normalized RQ values for the rostral CC of cuprizone recovery mice are indicative of the

Fig. 5 Immunohistochemical analysis of myelin oligodendrocyte glycoprotein (MOG) in coronal (a–l) and sagittal (m–x) sections through the CC of 2, 6, 12, and 16 month-old mice: control (a, d, g, j, m, p, s, and v), cuprizone (b, e, h, k, n, q, t, and w), cuprizone recovery (c, f, i, l, o, r, u, and x) mice. The boxes in m to r indicate the areas in the rostral CC shown in higher power in s to x, respectively. $n = 3$, bar in a = 100 μm (applies to a to l), bar in m = 100 μm (applies to m to r), bar in s = 100 μm (applies to s to x)



capacity of the tissue to increase myelin gene expression during the 3 weeks the mice were fed normal mouse chow, with any increases in myelin gene expression by cells in the rostral CC being an attempt to recover from the cuprizone-induced demyelination. Bonferroni's post-test revealed that the *MOG* normalized RQ values for the rostral CC of cuprizone recovery mice were significantly higher at 2 (0.72 ± 0.06), 12 (0.76 ± 0.08), and 16 (0.90 ± 0.13) months of age compared to age-matched cuprizone mice (0.33 ± 0.02 , 0.31 ± 0.08 , and 0.51 ± 0.08 , respectively) ($P < 0.05$) (Fig. 6a). Thus, there was approximately a

1.8-fold (16 months of age) to 2.5-fold (12 months of age) increase in *MOG* gene expression by cells of the rostral CC in cuprizone recovery mice compared to cuprizone mice. The *MOG* normalized RQ values for 12 (0.76 ± 0.08) and 16 (0.90 ± 0.13) month-old cuprizone recovery mice were also significantly higher than those for age-matched (0.33 ± 0.04 and 0.24 ± 0.01 , respectively) control mice ($P < 0.05$), increases that were approximately 2.3- and 3.8-fold higher, respectively (Fig. 6a). Thus, there were significant increases in *MOG* expression during the 3 weeks after switching the mice from a cuprizone-containing diet

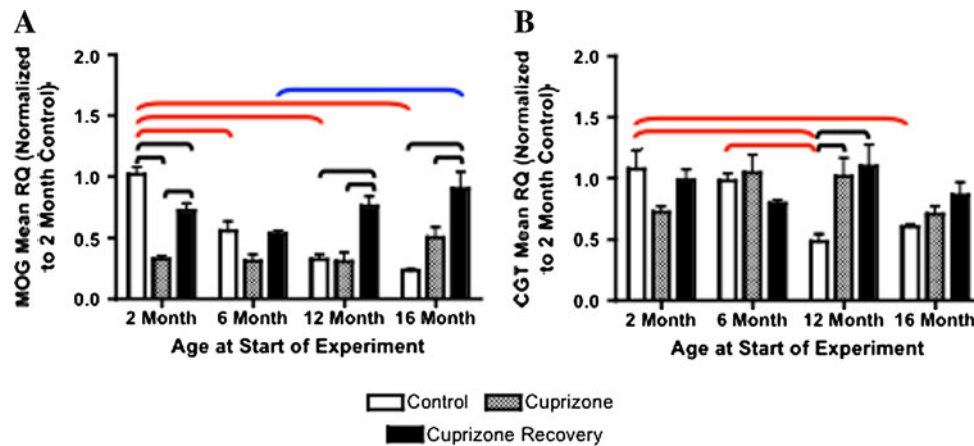


Fig. 6 Histograms depicting the gene expression profiles (quantitative [q] RT-PCR) for *MOG* **a**, and *CGT* **b** in the rostral CC of 2–16 month-old control, cuprizone and cuprizone recovery mice. Three mice were used for each treatment and for each age. The qRT-PCR data are expressed as normalized RQ values, with all RQ values for a gene being normalized to the mean RQ value of the respective

2-month-old control mice. The brackets in color denote significant age-related differences within a group (*red* = control, *blue* = cuprizone recovery), whereas black brackets denote significant treatment-related differences (Bonferroni's post-test; significance level of $P \leq 0.05$). For interpretation of the references to color in this figure legend, the reader is referred to the web version of the article

to one of normal mouse chow, even in mice as old as 16 months of age. In fact, the level of *MOG* gene expression in 16 month-old cuprizone recovery mice (0.90 ± 0.13) was significantly higher than that seen in 6 month-old cuprizone recovery mice (0.53 ± 0.02) ($P < 0.05$) (Fig. 6a). We interpret this significantly increased level of *MOG* gene expression in 16 month-old cuprizone recovery mice as evidence the tissue has retained a potential for myelin repair in spite of the drastic (i.e., 4-fold) reduction in *MOG* gene expression seen in the rostral CC of age-matched control mice.

With respect to *CGT* expression in the rostral CC of cuprizone recovery mice, the only significant difference in gene expression levels after 3 weeks of recovery from the demyelinating effects of a cuprizone-containing diet were seen at 12 months of age (1.10 ± 0.18) compared to age-matched control (0.48 ± 0.06) mice ($P < 0.05$) (Fig. 6b). This increased expression of *CGT* in the 12 month-old cuprizone recovery mice appears to be a transient tissue response, however, as the expression level in 16 month-old cuprizone recovery (0.86 ± 0.10) mice was not significantly different from that of age-matched control mice (0.60 ± 0.02) ($P > 0.05$). Thus, unlike what was seen with respect to *MOG* expression, not only did the age of the mouse have less of an effect on *CGT* expression in control mice, but the expression levels at each age also were less affected both by the cuprizone-induced demyelination as well as by a subsequent 3-week recovery period on normal mouse chow. There were no age-related differences in *CGT* gene expression in the rostral CC of cuprizone recovery mice ($P > 0.05$) (Fig. 6b), thus showing that expression of the *CGT* gene in response to recovery from cuprizone-induced demyelination was similar at all four ages.

No Change in Densities of Hoechst+ve Nuclei (Total Cell Numbers) During Normal Aging

The number of Hoechst+ve nuclei was counted in each of three digital images captured from the medial aspect of the rostral CC and the data were expressed as the number of Hoechst+ve nuclei per $500 \mu\text{m}^2$ (Fig. 7a). Hoechst dye will stain all cell nuclei and thus label all cells in the tissue section. There were no age-related differences in the density of Hoechst+ve nuclei in the rostral CC of mice fed the control diet (Bonferroni's post-test; $P > 0.05$). There was, in fact, minimal variation in the average density of Hoechst+ve nuclei over the four age groups of control mice (Fig. 7b, c); the densities varied from a low of 105.6 ± 2.7 at 12 months of age to a high of 114.6 ± 2.9 at 6 months of age, a difference of only nine nuclei (Figs. 7a). Thus, the significant main effect of age that was revealed by the two-way ANOVA (see Table 2) was not due to changes in total cell density during normal aging (i.e., in control mice).

Changes in Densities of Hoechst+ve Nuclei (Total Cell Numbers) in Response to Cuprizone-Induced Demyelination

Bonferroni's post-test revealed there was a significant difference in the density of Hoechst+ve nuclei in the rostral CC between age-matched control and cuprizone mice only at 2 months of age ($P < 0.05$) (Fig. 7a); the magnitude of the differences in total cell density was considerably less in 6–16 month-old mice, such that these differences failed to reach statistical significance ($P > 0.05$). For example, in 2 month-old mice the density of Hoechst+ve nuclei in the

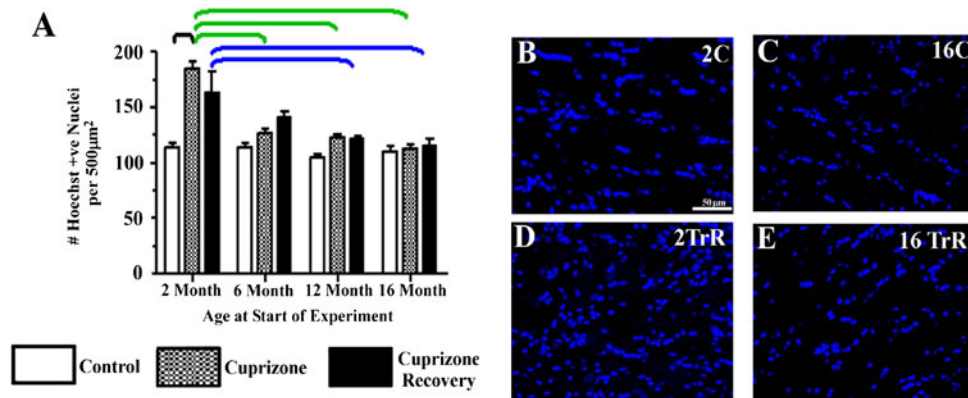


Fig. 7 a Histogram depicting the mean number (±SEM) of Hoechst+ve nuclei in the rostral CC of 2–16 month-old control, cuprizone and cuprizone recovery mice. Three mice were used for each treatment and for each age. The brackets in color denote significant age-related differences within a group (green = cuprizone, blue = cuprizone recovery), whereas black brackets denote significant treatment-related differences (Bonferroni's post-test; significance

rostral CC of cuprizone mice (185.0 ± 6.9) was approximately 62% higher than that of age-matched control mice (114.1 ± 3.6) ($P < 0.05$), whereas there was only a 10.6% (126.8 ± 4.0 ; 6 months old), 16.6% (123.1 ± 3.1 ; 12 months old) and 2.1% (113.2 ± 3.4 ; 16 months old) nonsignificant higher density of Hoechst+ve nuclei in older cuprizone mice compared to age-matched control (114.6 ± 2.9 , 105.6 ± 2.7 , 110.9 ± 4.8 , respectively) mice ($P > 0.05$).

In contrast to control mice, age-related differences in the density of Hoechst+ve nuclei were seen in the rostral CC of cuprizone mice ($P < 0.05$). In the older mice, the tissue response to cuprizone-induced demyelination generated significantly lower total numbers of cells per unit area compared to the tissue response in younger mice (Fig. 7a). The average density of Hoechst+ve nuclei per $500 \mu\text{m}^2$ in the rostral CC of cuprizone mice declined from a high of 185.0 ± 6.9 at 2 months of age to a low of 113.2 ± 3.4 at 16 months of age ($P < 0.05$). The differential effect of age on total cell density after cuprizone-induced demyelination vs normal aging is one reason why the ANOVA revealed a significant interaction effect (see Table 2).

Changes in Densities of Hoechst+ve Nuclei (Total Cell Numbers) After 3 Weeks of Recovery from Cuprizone-Induced Demyelination

A significant difference in density of Hoechst+ve nuclei was seen when cuprizone recovery mice were compared to age-matched control mice, but only at 2 months of age ($P < 0.05$) (Fig. 7a). As was found for the cuprizone mice, the magnitude of the differences in total cell density was considerably less in 6–16 month-old cuprizone recovery mice, such that in comparison to total cell densities in

level of $P < 0.05$). **b–e** Hoechst+ve nuclei in coronal sections of CC from a 2 month-old (2C) control mouse **b**, a 16 month-old (16C) control mouse **c**, a 2 month-old (2TrR) cuprizone recovery mouse **d** and a 16 month-old (16TrR) cuprizone recovery mouse **e**. Bar in **b** = $50 \mu\text{m}$ (applies to **b–e**). For interpretation of the references to color in this figure legend, the reader is referred to the web version of the article

age-matched control mice they failed to reach statistical significance ($P > 0.05$). Compared to age-matched control mice, the density of Hoechst+ve nuclei in cuprizone recovery mice at 2 months of age (162.7 ± 19.8) was approximately 42.6% higher than that of age-matched control mice (114.1 ± 3.6) ($P < 0.05$), whereas the total cell densities in older cuprizone recovery mice were only 22.9% (140.9 ± 6.0 ; 6 months of age), 14.9% (121.3 ± 2.7 ; 12 months of age), and 4.0% (115.3 ± 7.2 ; 16 months of age) higher compared to age-matched control (114.6 ± 2.9 , 105.6 ± 2.7 , and 110.9 ± 4.8 , respectively) mice ($P > 0.05$).

Similar to the cuprizone mice, age-related differences in the density of Hoechst+ve nuclei were also seen in the rostral CC of cuprizone recovery mice ($P < 0.05$). In the older mice, the tissue response during recovery from cuprizone-induced demyelination generated significantly lower total numbers of cells per unit area compared to the tissue response in younger mice (Fig. 7a). For the cuprizone recovery mice, the average density of Hoechst+ve nuclei declined from a high of 162.7 ± 19.8 in 2 month-old mice to a low of 115.3 ± 7.2 at 16 months of age (Fig. 7a, d, e). This differential effect of age on total cell density after 3 weeks recovery from cuprizone-induced demyelination versus normal aging is another reason why the ANOVA had revealed a significant interaction effect between age and treatment (see Table 2).

Changes in *PDGFαR*, *Olig2*, and *Nkx2.2* Gene Expression during Normal Aging

We next asked whether there were age-related changes in expression of the *PDGFαR* gene (expressed by glial

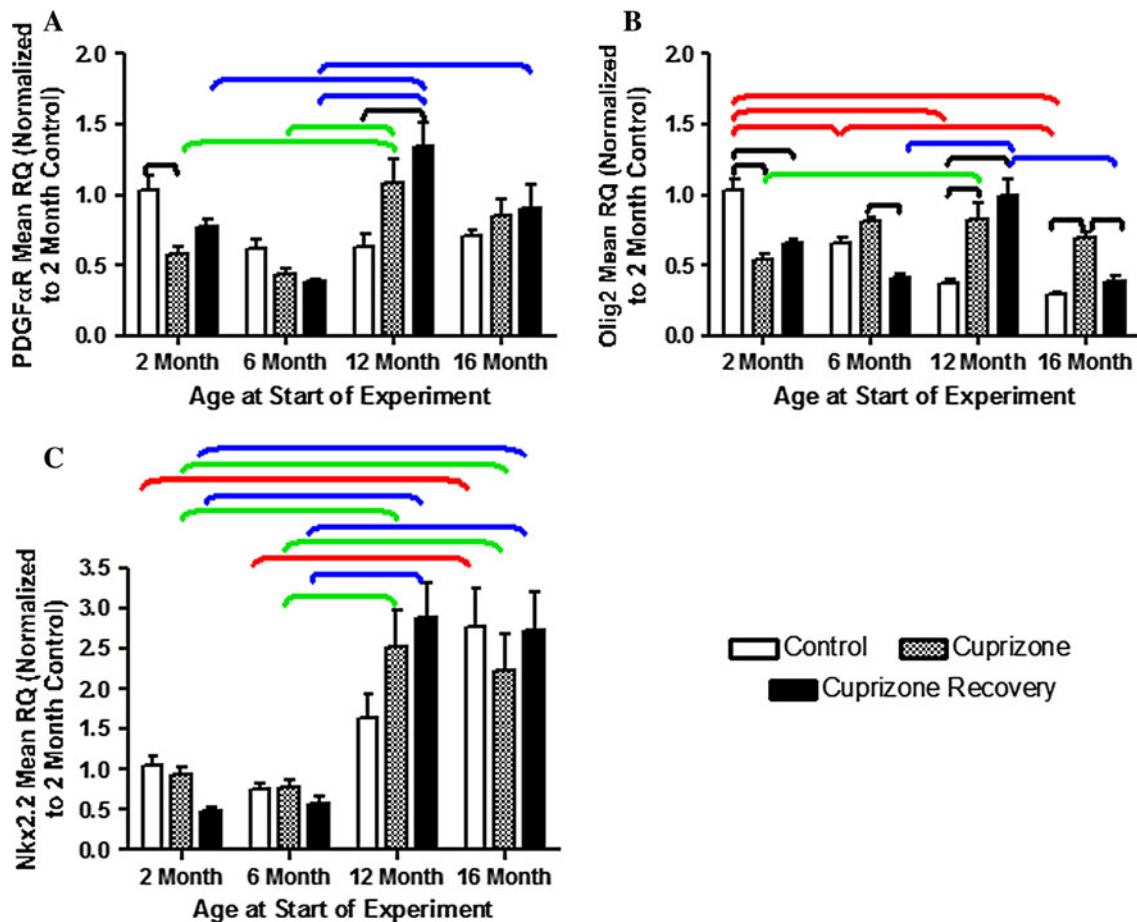


Fig. 8 Histograms depicting the gene expression profiles (quantitative [q] RT-PCR) for *PDGFαR* **a**, *Olig2* **b**, and *Nkx2.2* **c** in the rostral CC of 2–16 month-old control, cuprizone and cuprizone recovery mice. Three mice were used for each treatment and for each age. The qRT-PCR data are expressed as normalized RQ values, with all RQ values for a gene being normalized to the mean RQ value of the respective 2-month-old control mice. The brackets in color denote

significant age-related differences within a group (*red* = control, *green* = cuprizone, *blue* = cuprizone recovery), whereas black brackets denote significant treatment-related differences (Bonferroni's post-test; significance level of $P \leq 0.05$). For interpretation of the references to color in this figure legend, the reader is referred to the web version of the article

progenitor cells, including OL progenitors) or of the genes for the *Olig2* and *Nkx2.2* TFs (involved in the differentiation of OLs) in the rostral CC. For the gene expression analysis, the RQ values of *PDGFαR*, *Olig2*, and *Nkx2.2* genes were normalized to the respective mean *PDGFαR*, *Olig2*, and *Nkx2.2* RQ values of 2-month-old control mice, as described previously for *MOG* and *CGT*. The statistical significance of age- and treatment-related differences in normalized RQ values for each gene was assessed using two-way ANOVAs (see Table 2).

There were no age-related changes in gene expression of *PDGFαR* in the 2–16 month-old control mice ($P > 0.05$) (Fig. 8a). However, Bonferroni's post-test revealed a significant age-related decreased expression of *Olig2* in the rostral CC of these control mice (Fig. 8b). The normalized RQ value of *Olig2* at 16 months of age (0.30 ± 0.02) was more than 3-fold lower than that of 2 month-old mice (1.0 ± 0.08) ($P < 0.05$). In contrast, Bonferroni's post-test

on the normalized *Nkx2.2* RQ values revealed significant age-related increases in gene expression in the rostral CC of control mice (Fig. 8c). The normalized *Nkx2.2* RQ values at 16 months of age (2.78 ± 0.47) were close to 2.6-fold higher than in 2 month-old (1.06 ± 0.11) control mice ($P < 0.05$) and close to 3.8-fold higher than in 6 month-old (0.74 ± 0.09) control mice ($P < 0.05$). Thus, age differentially affected expression of the *Olig2* and *Nkx2.2* genes, resulting by 16 months of age in a 3-fold reduction in expression of the *Olig2* gene and a 2.6-fold increase in expression of *Nkx2.2*.

Changes in *PDGFαR*, *Olig2*, and *Nkx2.2* Gene Expression in Response to Cuprizone-Induced Demyelination

Compared to control mice, the cuprizone-induced demyelination affected *PDGFαR* gene expression by glial

progenitor cells in the rostral CC only in 2 month-old mice. There was a significantly decreased expression of the *PDGF α R* gene in 2 month-old cuprizone (0.58 ± 0.05) versus control (1.0 ± 0.1) mice ($P < 0.05$) (Fig. 8a), but the differences in normalized RQ values at 6–16 months of age failed to reach statistical significance ($P > 0.05$) (Fig. 8a). Although we did not find any age-related changes in gene expression of *PDGF α R* in the 2–16 month-old control mice ($P > 0.05$), we did find age-related increases in *PDGF α R* expression in the rostral CC of cuprizone mice (Fig. 8a). The level of *PDGF α R* gene expression in the rostral CC of 12 month-old cuprizone mice (1.08 ± 0.17) was almost 2-fold higher than in 2 month-old cuprizone mice (0.58 ± 0.05) ($P < 0.05$).

With respect to the *Olig2* gene, Bonferroni's post-test revealed that in response to cuprizone-induced demyelination the normalized RQ values for *Olig2* were significantly higher in 12 (0.83 ± 0.11) and 16 (0.70 ± 0.04) month-old cuprizone mice compared to age-matched control (0.37 ± 0.04 and 0.3 ± 0.02 , respectively) mice ($P < 0.05$) (Fig. 8b). In the 2 month-old cuprizone mice however, the expression levels of *Olig2* were significantly decreased by almost 50% (0.54 ± 0.04) compared to age-matched control (1.0 ± 0.08) mice ($P < 0.05$). When age-related changes in *Olig2* gene expression following cuprizone treatment were assessed with Bonferroni's post-test there was a significantly higher level of *Olig2* gene expression at 12 months of age (0.83 ± 0.11) compared to 2 month-old cuprizone (0.54 ± 0.04) mice ($P < 0.05$) (Fig. 8b).

None of the differences in normalized RQ values for the *Nkx2.2* gene between control and cuprizone mice were large enough to reach statistical significance ($P > 0.05$) (Fig. 8c), indicating that age was the primary factor determining expression levels of this gene. Bonferroni's post-test on these normalized *Nkx2.2* RQ values revealed significant age-related increases in gene expression by cells in the rostral CC of cuprizone mice (Fig. 8c). The normalized RQ values at both 12 (2.53 ± 0.45) and 16 (2.24 ± 0.44) months of age in the cuprizone mice were more than 2-fold higher than the normalized RQ values in 2 month-old (0.95 ± 0.08) cuprizone mice ($P < 0.05$).

Changes in *PDGF α R*, *Olig2*, and *Nkx2.2* Gene Expression After 3 Weeks of Recovery from Cuprizone-Induced Demyelination

There were no significant differences in *PDGF α R* normalized RQ values between cuprizone and cuprizone recovery mice at any of the ages ($P > 0.05$) (Fig. 8a). There was, however, significantly increased *PDGF α R* gene expression in the rostral CC of 12 month-old cuprizone recovery (1.35 ± 0.16) versus aged-matched control

(0.64 ± 0.09) mice ($P < 0.05$) (Fig. 8a). Furthermore, there were also age-related increases in *PDGF α R* gene expression in the rostral CC of cuprizone recovery mice. The level of *PDGF α R* gene expression in the rostral CC of cuprizone recovery mice was significantly higher at 12 months of age (1.35 ± 0.16) compared to 2 month-old (0.77 ± 0.05) and 6 month-old (0.38 ± 0.02) cuprizone recovery mice ($P < 0.05$) (Fig. 8a). In addition, the level of *PDGF α R* gene expression in the rostral CC of 16 month-old cuprizone recovery mice (0.91 ± 0.17) was significantly higher compared to 6 month-old (0.38 ± 0.02) cuprizone recovery mice ($P < 0.05$).

For the *Olig2* gene, expression levels were significantly decreased in cuprizone recovery mice at both 6 (0.41 ± 0.03) and 16 (0.39 ± 0.04) months of age compared to 6 (0.81 ± 0.03) and 16 (0.70 ± 0.04) month-old cuprizone mice ($P < 0.05$) (Fig. 8b). In addition, Bonferroni's post-test revealed a significantly decreased level of *Olig2* expression in the rostral CC of 2 month-old cuprizone recovery mice (0.65 ± 0.04) compared to age-matched control mice (1.0 ± 0.08), but a significantly increased level of *Olig2* expression in 12 month-old cuprizone recovery mice (1.0 ± 0.12) compared to age-matched control mice (0.37 ± 0.04) ($P < 0.05$). The level of *Olig2* gene expression was also significantly higher in 12 month-old cuprizone recovery mice (1.0 ± 0.12) compared to both 6 month-old (0.41 ± 0.03) and 16 month-old (0.39 ± 0.04) cuprizone recovery mice ($P < 0.05$) (Fig. 8b).

None of the differences in normalized RQ values for the *Nkx2.2* gene between cuprizone recovery and either age-matched control or cuprizone mice were large enough to reach statistical significance ($P > 0.05$) (Fig. 8c). Bonferroni's post-test on the normalized *Nkx2.2* RQ values did reveal however, significant age-related increases in gene expression in the rostral CC of cuprizone recovery mice (Fig. 8c). The age-related increases in the levels of *Nkx2.2* gene expression were substantial in cuprizone recovery mice, where the level of expression was 5- to 6-fold higher in the rostral CC at 12 (2.89 ± 0.42) and 16 (2.72 ± 0.49) months of age compared to 2 month-old (0.48 ± 0.05) cuprizone recovery mice ($P < 0.05$). Thus, as was seen for *Nkx2.2* gene expression in control and cuprizone mice, age was the primary factor driving expression of this gene in the cuprizone recovery mice.

Changes in Density of Cells of the OL Lineage After Cuprizone-Induced Demyelination

The *Olig2* protein functions as a TF in cells of the OL lineage, where it plays a role in specification, differentiation and maturation of OLs (Nicolay et al. 2007). In all cells of the OL lineage, from OL progenitor cells to myelinating OLs, *Olig2* is localized to the nucleus (Zhao

et al. 2009). Cytoplasmic translocation of Olig2 has been shown to result in the progenitor cells differentiating down the astrocyte pathway (Cassiani-Ingoni et al. 2006; Magnus et al. 2007; Zhao et al. 2009). Therefore, when computing the cell counts of Olig2+ve cells from the immunostained sections, cell count data per 500 μm^2 were collected separately for nuclear [Olig2^{Nuc}+ve cells] versus cytoplasmic [Olig2^{Cyto}+ve cells] localization of Olig2 in tissue sections that were double-labeled, respectively, with OL or astrocyte-specific marker proteins.

Tissue sections double immunostained with antibodies to the astrocyte-specific intermediate filament protein GFAP and to the TF Olig2 were used to count the number of Olig2^{Nuc}+ve/GFAP–ve cells (Fig. 9a, d) per 500 μm^2 . These GFAP–ve cells with nuclear localization of Olig2 are OL lineage cells encompassing cells of the lineage from the OL progenitor cells through to myelinating OLs. Cell counts of Olig2^{Nuc}+ve/PDGFR+ve (Fig. 9b, e) in tissue sections double immunostained with these two antibodies provided cell density data for OL progenitor cells in the rostral CC of the different treatment groups. Finally, cells that were PDGFR+ve/GFAP–ve (Fig. 9c, f) represented PDGFR+ve glial progenitor cells that had not yet made a fate choice of differentiating into astrocytes. Hence the statistical analyses focused on the density of glial progenitor (PDGFR+ve/GFAP–ve), OL progenitor (Olig2^{Nuc}+ve/PDGFR+ve), and OL lineage cells (Olig2^{Nuc}+ve/

GFAP–ve). To compare the effect of treatment on the cell densities of each of these cell populations in the rostral CC of the mice, separate two-way ANOVA's were done for each age of mouse (see Table 2). The independent variables for these statistical analyses were the phenotype of the cells (e.g. Olig2^{Nuc}+ve/GFAP–ve) and the treatment. Thus, the intent with this statistical analysis was a comparison of the effect of treatment on the density of each of the three cell phenotypes at a single age, as opposed to a statistical evaluation of age-related differences in the density of each cell phenotype.

Bonferroni's post-test on the cell density data at 2 months of age revealed a significant 4.2- to 3.1-fold increase in the density of glial progenitor cells (PDGFR+ve/GFAP–ve) in both the cuprizone (16.0 \pm 3.35) and cuprizone recovery (11.59 \pm 2.04) mice, respectively, compared to that of 2-month-old control mice (3.78 \pm 0.61) ($P < 0.05$) (Fig. 10a). At 6, 12, and 16 months of age, however, there were no statistically significant cuprizone-induced increases in glial progenitor cell density ($P > 0.05$) (Figs. 10b–d). There were also no treatment-related differences in the density of OL progenitor cells (Olig2^{Nuc}+ve/PDGFR+ve) at any of the ages ($P > 0.05$) (Fig. 10a–d).

The post-test also revealed the density of OL lineage cells (Olig2^{Nuc}+ve/GFAP–ve) in the 2 month-old control (20.27 \pm 3.05) mice was 8.2- and 2.3-fold higher than that

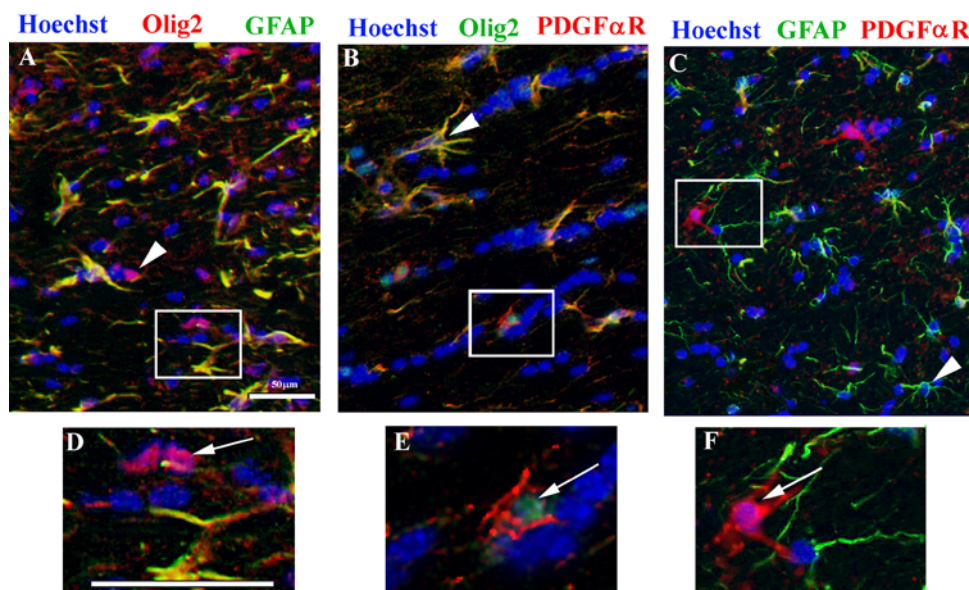


Fig. 9 Immunohistochemical analysis of Olig2^{Nuc}+ve/GFAP–ve cells (**a**, **d**), Olig2^{Nuc}+ve/PDGFR+ve cells (**b**, **e**), PDGFR+ve/GFAP–ve cells (**c**, **f**) in coronal sections through the rostral CC. The images were obtained from CC of 6 month-old cuprizone (**a**, **d**), cuprizone recovery (**b**, **e**), and control (**c**, **f**) mice. The white boxed area in **a–c** denote the portion of each image that is shown at higher magnification in **d–f**, respectively. **d** Two Olig2^{Nuc}+ve/GFAP–ve

cells in the top center of the image (*arrow*). **e** A Olig2^{Nuc}+ve/PDGFR+ve cell in the center of the image (*arrow*). **f** A PDGFR+ve/GFAP–ve cell on the left side of the image (*arrow*). The arrowhead in **a** points out an Olig2^{Cyto}+ve/GFAP–ve cell, in **b** points out a Olig2^{Cyto}+ve/PDGFR+ve cell, and in **c** points out a PDGFR–ve/GFAP+ve astrocyte. bar (**a**, **d**) = 50 μm , $n = 3$

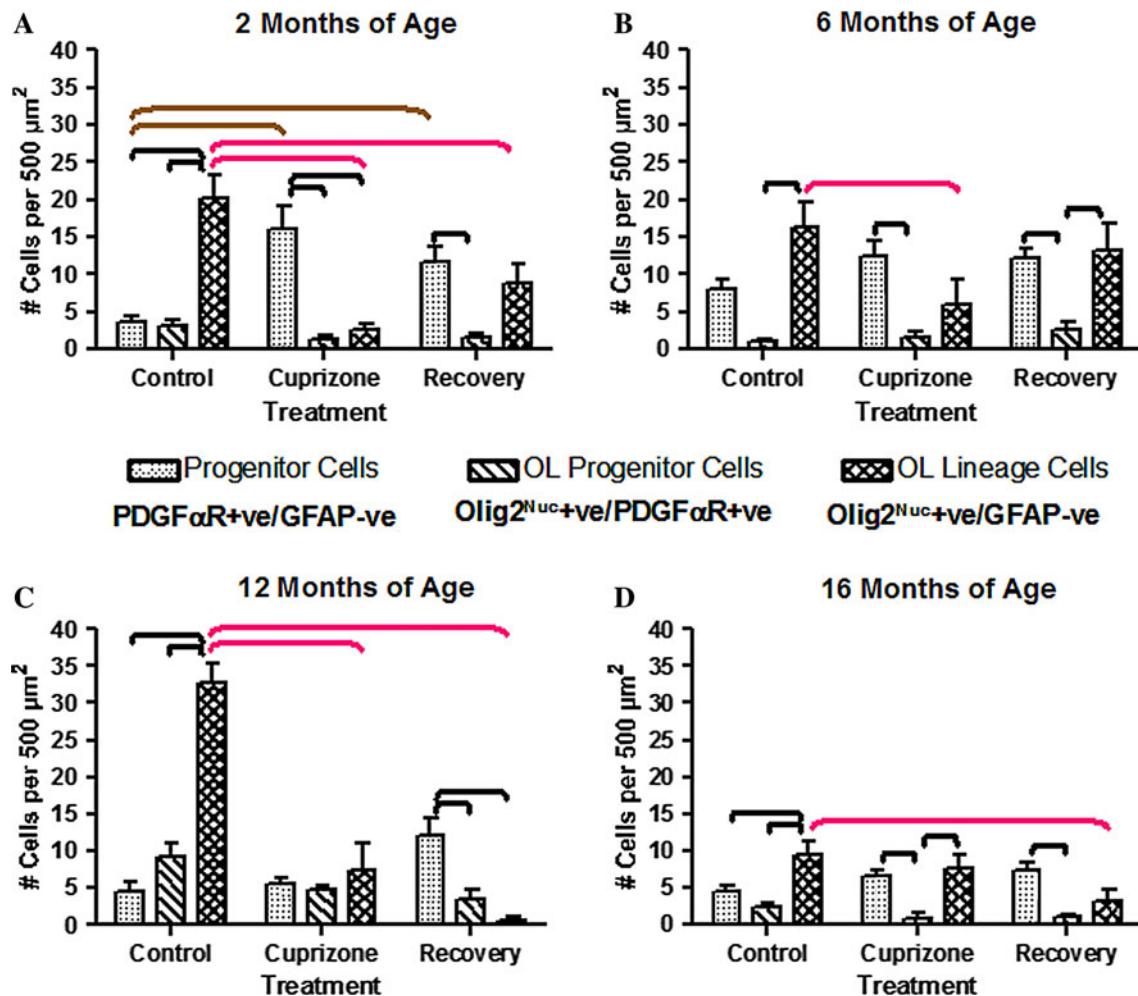


Fig. 10 Histograms depicting the mean number (\pm SEM) of progenitor (PDGF α R+ve/GFAP-ve), OL progenitor (Olig2^{Nuc}+ve/PDGF α R+ve), and OL lineage (Olig2^{Nuc}+ve/GFAP-ve) cells in the rostral CC of 2 (a), 6 (b), 12 (c), and 16 (d) month-old control, cuprizone and cuprizone recovery mice. Three mice were used for each treatment and for each age. The brackets in color denote

significant differences within a phenotype (brown = progenitor cells, pink = OL lineage cells), whereas black brackets denote significant differences between phenotypes (Bonferroni's post-test; significance level of $P \leq 0.05$). For interpretation of the references to color in this figure legend, the reader is referred to the web version of the article

seen in the cuprizone (2.48 ± 0.88) and cuprizone recovery (8.83 ± 2.44) mice, respectively ($P < 0.05$) (Fig. 10a). In the rostral CC of 6 month-old mice there was a significant 2.7-fold decrease in the density of OL lineage cells in the cuprizone (5.98 ± 3.41) mice compared to age-matched control (16.28 ± 3.41) mice ($P < 0.05$) (Fig. 10b). The density of OL lineage cells also showed a significant treatment-related decrease in the 12 month-old mice (Fig. 10c), with the density of these cells being 4.4- and 49-fold lower in cuprizone and cuprizone recovery mice, respectively, compared to age-matched control mice ($P < 0.05$). At 16 months of age, the cell density of OL lineage cells in control mice was significantly higher than that of age-matched cuprizone recovery mice ($P < 0.05$) (Fig. 10d).

Changes in Density of Cells of the Astrocyte Lineage After Cuprizone-Induced Demyelination

Tissue sections double immunostained with antibodies to the astrocyte-specific intermediate filament protein GFAP and to the TF Olig2 were used to count the number of Olig2^{Cyto}+ve/GFAP+ve cells and Olig2^{Cyto}-ve/GFAP+ve cells (Fig. 9) per $500 \mu\text{m}^2$. The Olig2^{Cyto}-ve/GFAP+ve cells are mature astrocytes in the rostral CC. Olig2^{Cyto}+ve/GFAP+ve cells are newly formed astrocytes that are formed following translocation of Olig2 protein from the nucleus to the cytoplasm. Finally, cell counts of Olig2^{Cyto}+ve/PDGF α R+ve (Fig. 9) in tissue sections double immunostained with these two antibodies provided cell density data for progenitor cells that made a fate choice

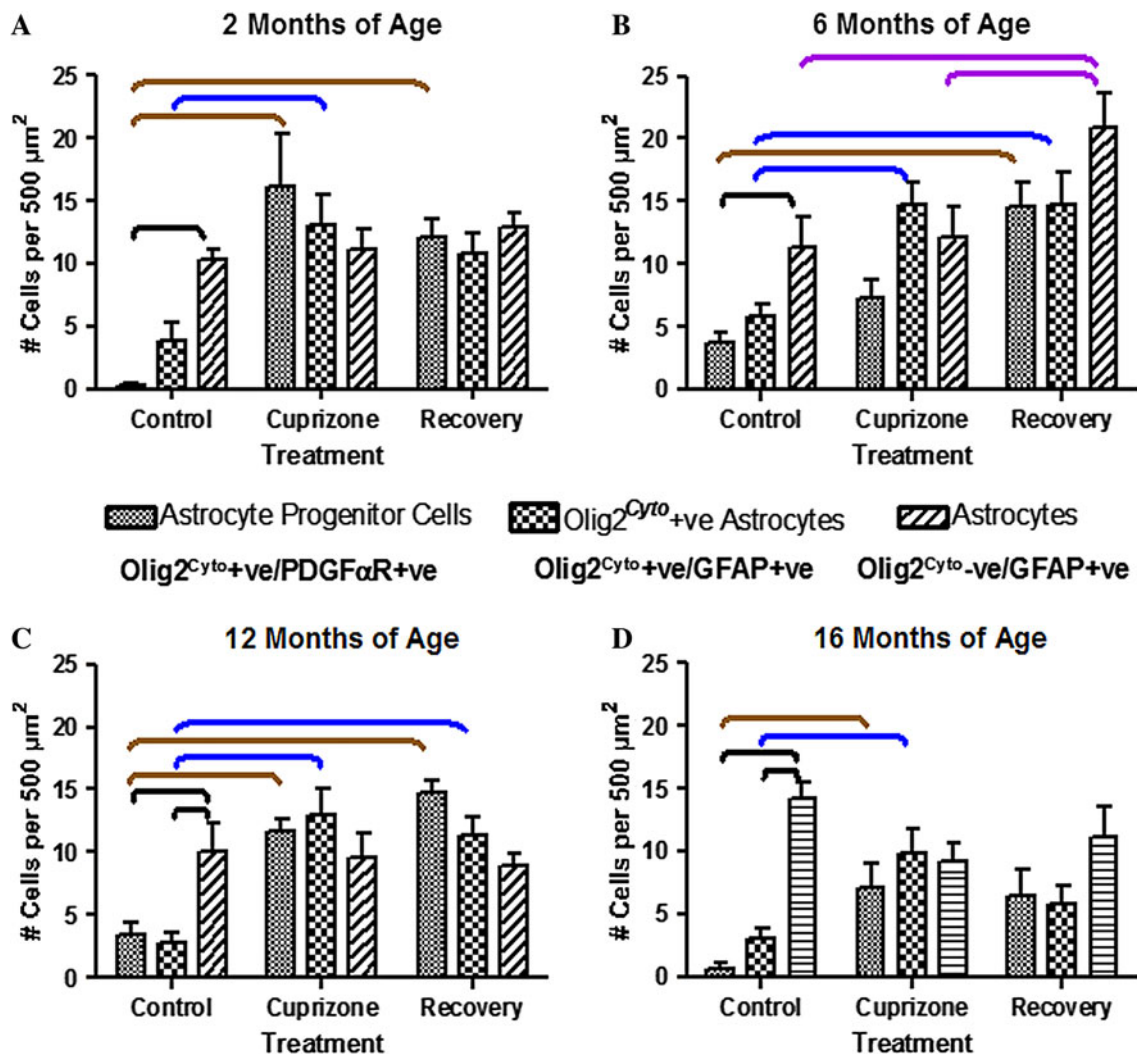


Fig. 11 Histograms depicting the mean number (\pm SEM) of astrocyte progenitor cells (Olig2^{Cyto}+ve/PDGF α R+ve), newly formed astrocytes (Olig2^{Cyto}+ve/GFAP+ve), and mature astrocytes (Olig2^{Cyto}-ve/GFAP+ve) in the rostral CC of 2 (a), 6 (b), 12 (c), and 16 (d) month-old control, cuprizone and cuprizone recovery mice. Three mice were used for each treatment and for each age. The brackets in

color denote significant differences within a phenotype (brown = astrocyte progenitor cells, blue = Olig2^{Cyto}+ve astrocytes, purple = astrocytes), whereas black brackets denote significant differences between phenotypes (Bonferroni's post-test; significance level of $P \leq 0.05$). For interpretation of the references to color in this figure legend, the reader is referred to the web version of the article

to differentiate into astrocytes (i.e., astrocyte progenitor cells), as indicated by the cytoplasmic translocation of the Olig2 protein.

To compare the effect of age and treatment on the cell densities of each of these cell populations in the rostral CC of the mice, separate two-way ANOVA's were done for each age of mouse (see Table 2). The independent variables for these statistical analyses were the phenotype of the cells (e.g. Olig2^{Cyto}+ve/GFAP+ve) and the treatment. Thus, the intent with this statistical analysis was a comparison of the effect of treatment on the density of each of the three astrocyte cell phenotypes at a single age, as opposed to an evaluation of age-related statistical differences in the density of each cell phenotype. Astrocytes will

respond to any age-related or cuprizone-induced tissue damage to CNS white matter, and as a consequence of the subsequent gliosis the density of astrocytes and their progenitors in the rostral CC should increase in accordance with the extent of the astrocytic response.

Bonferroni's post-test on these cell density data at 2 months of age revealed a huge 42- to 32-fold increase in the density of Olig2^{Cyto}+ve/PDGF α R+ve astrocyte progenitor cells in both the cuprizone (16.1 ± 4.22) and cuprizone recovery (12.2 ± 1.50) mice, respectively, compared to that of 2 month-old control mice (0.38 ± 0.16) ($P < 0.05$) (Fig. 11a). The post-test also revealed the density of Olig2^{Cyto}+ve/GFAP+ve astrocytes in the 2 month-old cuprizone (13.06 ± 2.44) mice was 3.3-fold higher than that seen in the

control (3.93 ± 1.33) mice ($P < 0.05$) (Fig. 11a). There were no significant treatment-related differences in the density of Olig2^{Cyto}-ve/GFAP+ve astrocytes in these 2 month-old mice ($P > 0.05$). Thus, at 2 months of age the treatment-related effects on density of cells of the astrocyte lineage were confined to the Olig2^{Cyto}+ve/PDGFR+ve astrocyte progenitor cells and Olig2^{Cyto}+ve/GFAP+ve newly formed astrocytes in the rostral CC.

In the rostral CC of 6 month-old mice there was a significant increase in the density of Olig2^{Cyto}+ve/PDGFR+ve astrocyte progenitor cells only in the cuprizone recovery mice (14.59 ± 1.96) compared to age-matched control (3.72 ± 0.87) mice ($P < 0.05$) (Fig. 11b). Treatment-related differences were also seen in the density of Olig2^{Cyto}+ve/GFAP+ve astrocytes in the 6 month-old mice, with cell densities in the cuprizone (14.80 ± 1.76) and cuprizone recovery (14.78 ± 2.50) mice being 2.5-fold higher than that seen in control (5.89 ± 0.96) mice ($P < 0.05$). Although there was no significant difference in the density of Olig2^{Cyto}-ve/GFAP+ve mature astrocytes in the rostral CC of 6 month-old control (11.37 ± 2.50) and cuprizone-fed (12.17 ± 2.40) mice ($P > 0.05$), both of these were significantly lower than the Olig2^{Cyto}-ve/GFAP+ve mature astrocyte cell density seen in 6 month-old cuprizone recovery mice (20.93 ± 2.69) ($P < 0.05$). Thus, in contrast to that seen in 2 month-old mice, treatment-related effects on density of cells of the astrocyte lineage involved all three populations of cells that were quantified.

Similar to the 2-month-old mice, in the rostral CC of 12-month-old mice there was a significant increase in the density of Olig2^{Cyto}+ve/PDGFR+ve astrocyte progenitor cells in both the cuprizone (11.70 ± 0.97) and cuprizone recovery (14.73 ± 0.97) mice, respectively, compared to that of 12 month-old control mice (3.43 ± 0.96) ($P < 0.05$) (Fig. 11c). Treatment-related differences were also seen in the density of Olig2^{Cyto}+ve/GFAP+ve newly formed astrocytes in the 12 month-old mice, with cell densities in the cuprizone (12.96 ± 2.17) and cuprizone recovery (11.44 ± 1.43) mice being, respectively, 4.6- and 4.0-fold higher than that seen in the control (2.83 ± 0.86) mice ($P < 0.05$). There were no significant differences in the density of Olig2^{Cyto}-ve/GFAP+ve mature astrocytes in the rostral CC of 12 month-old control (10.14 ± 2.21), cuprizone-fed (9.63 ± 1.92), and cuprizone recovery (8.97 ± 0.88) mice ($P > 0.05$). Thus, in contrast to those seen in 6 month-old mice, treatment-related effects on density of cells of the astrocyte lineage at 12 months of age involved only the Olig2^{Cyto}+ve/PDGFR+ve astrocyte progenitor cells and the Olig2^{Cyto}+ve/GFAP+ve newly formed astrocytes.

Bonferroni's post-test on the astrocyte lineage cell density data at 16 months of age revealed a 9.7-fold increase in the density of Olig2^{Cyto}+ve/PDGFR+ve astrocyte progenitor

cells in the cuprizone mice (7.07 ± 2.01) compared to that of 16 month-old control mice (0.73 ± 0.34) ($P < 0.05$) (Fig. 11d). The post-test also revealed the density of Olig2^{Cyto}+ve/GFAP+ve newly formed astrocytes in the 16 month-old cuprizone (9.83 ± 2.04) mice was almost 3.2-fold higher than that seen in the control (3.12 ± 0.79) mice ($P < 0.05$) (Fig. 11d). There were no significant treatment-related differences in the density of Olig2^{Cyto}-ve/GFAP+ve mature astrocytes in these 16 month-old mice ($P > 0.05$). Thus, in common with the findings at 2 and 12 months of age, the treatment-related effects on density of cells of the astrocyte lineage were confined to the Olig2^{Cyto}+ve/PDGFR+ve astrocyte progenitor and Olig2^{Cyto}+ve/GFAP+ve newly formed astrocytes in the rostral CC.

Discussion

The age-related decreased efficiency of OL myelination and remyelination is due to impaired recruitment and differentiation of OL progenitor cells (Ando et al. 2003; Chari et al. 2003; Franklin et al. 2002; Peters 2002b; Rist and Franklin 2008; Sim et al. 2002). Changes in transcriptional control likely underlie this impaired recruitment of OL precursor cells into demyelinated lesions and/or the differentiation of these cells into myelinating glia (Franklin et al. 2002; Sim et al. 2002). The expression profiles of growth factors known to be important for oligodendrogenesis (i.e., PDGF, FGF, and TGF- β) are temporally delayed in older animals compared to young adults and this may also contribute to the slower recruitment and differentiation of OL precursor cells (Franklin et al. 2002; Hinks and Franklin 2000).

Our study showed that between 2 and 16 months of age there was a similar increase in day zero body weights for the controls, cuprizone, and cuprizone recovery mice, thus indicating the mice in all three groups began the study with comparable body weights (Fig. 3a). Mice on the cuprizone diet lost weight, compared to controls, with the size of the weight loss being influenced both by the age of the mouse and by how many weeks they had been on the cuprizone diet. Furthermore, the oldest mice did not recover as well, in terms of body weight gain, as did the younger mice (Fig. 3d), indicative perhaps of a slower recovery from the effects of being fed a cuprizone diet. In spite of the weight loss and the poorer weight gain seen in the older cuprizone recovery mice, the mice remained in good health for the duration of the study and thus age-related changes seen at the cellular level are occurring in otherwise healthy animals.

Our findings at the cellular level shed some light on possible explanations for the age-related decreased efficiency of myelination and remyelination. First, we showed that the age-related impaired recruitment of OL progenitor

cells occurs in spite of there being no major decrease in the size of the progenitor cell pool. The PDGF α R+ve/GFAP–ve progenitor and Olig2^{Nuc}+ve/PDGF α R+ve OL progenitor cell densities appeared to remain fairly constant across all four ages of control mice. Second, the PDGF α R+ve/GFAP–ve progenitor and Olig2^{Nuc}+ve/PDGF α R+ve OL progenitor cell densities showed no statistically significant increase in response to cuprizone-induced demyelination in the 6–16 month-old mice. However, there were significant cuprizone-induced increased densities of Olig2^{Cyto}+ve/PDGF α R+ve astrocyte progenitor cells in these same mice. The latter finding indicates that at least a portion of the PDGF α R+ve progenitor cell pool retains the ability to make a fate choice to differentiate into astrocytes, as occurs following cytoplasmic translocation of Olig2, even in mice as old as 16 months of age. Third, consistent with this view of a possible age-related switch in the fate choice of PDGF α R+ve progenitor cells that may begin as early as 2 months of age, was the finding of cuprizone-induced increases in density of Olig2^{Cyto}+ve/GFAP+ve newly formed astrocytes in the rostral CC of the 2–16 month-old mice. Cytoplasmic translocation of Olig2 in PDGF α R+ve progenitors results in differentiation down the astrocyte pathway (Cassiani-Ingoni et al. 2006; Magnus et al. 2007; Zhao et al. 2009). Therefore, Olig2^{Nuc}+ve cells are OLs whereas Olig2^{Cyto}+ve cells are astrocytes. Fourth, there was an age-related increased expression of the *Nkx2.2* TF in all treatment groups beginning at 12 months of age. In cells of the OL lineage, *Nkx2.2* functions as a transcriptional repressor (Tochitani and Hayashizaki 2008; Watanabe et al. 2004; Wei et al. 2005). Finally, with respect both to normal aging and to the tissue response to cuprizone-induced demyelination, it appears that the time between 12 and 16 months of age is a critical period during which there is an age-related decrease in the number of OL lineage cells (Olig2^{Nuc}+ve/GFAP–ve) in control mice and in the number of such cells in the rostral CC tissue of mice recovering from cuprizone-induced demyelination. The discussion that follows addresses each of these points in turn.

With respect to the rostral CC in control mice as old as 16 months of age, our findings suggest the decreased efficiency of myelination during normal aging is not due to decreased numbers of progenitor cells. In control mice the densities of both PDGF α R+ve/GFAP–ve progenitor cells and of Olig2^{Nuc}+ve/PDGF α R+ve OL progenitor cells remained fairly constant between 2 and 16 months of age. Rivers et al. (2008) also reported no change in the density of PDGF α R+ve cells in the rostral CC of control mice between the ages of 1.5–4.5 months of age. Our study thus extends the age range (up to 16 months of age) over which it can be stated that the numbers of PDGF α R+ve progenitor cells remain fairly constant.

The density of PDGF α R+ve/GFAP–ve progenitor cells increased significantly only in 2 month-old cuprizone mice compared to controls (Fig. 10a). This was also confirmed in another recent study where double transgenic mice (8–10 weeks old) which express tamoxifen-inducible CreER under the control of Olig2 promoter and a ROSA-EGFP reporter to trace the fate of Olig2+ve cells showed significant increases in NG2+ve/APC+ve OLs after cuprizone treatment (Islam et al. 2009). However, the absence of a cuprizone-induced increase in the density of PDGF α R+ve/GFAP–ve progenitor cells in mice older than 2 months of age would certainly impede the ability of the tissue to generate sufficient numbers of OLs for remyelinating axons in the rostral CC. In mice 12 and 16 months of age, we found the density of PDGF α R+ve/GFAP–ve progenitor cells in cuprizone mice was only 36% and 41%, respectively, compared to the cell density seen in 2 month-old cuprizone mice. According to Rivers et al. (2008), PDGF α R+ve cells have a cell cycle time of approximately 1 week and only about half of these cells are mitotic. Thus, the 6 week exposure to cuprizone should have been more than ample time to generate significantly increased numbers of PDGF α R+ve/GFAP–ve progenitor cells in the older mice, provided these cells comprised part of the proliferating pool of progenitor cells.

The study of Rivers et al. (2008) showed that almost one-third of the mature OLs present in the rostral CC of 8.5 month-old mice had been formed de novo between 1.5 and 8.5 months of age, and that at least some of these newly formed OLs had assembled a myelin sheath. Thus, there is a gradual increase in the number of OLs in the rostral CC over the first several months after birth, which is not surprising given the de novo myelination that is known to occur in this area in humans and in non-human primates (Bartzokis 2004b; Bartzokis et al. 2004a, b). Given this continual addition of new OLs to the cell population of the rostral CC as the mice get older (Rivers et al., 2008), it is no surprise that we found such a large increase in the density of cells of the OL lineage (i.e., Olig2^{Nuc}+ve/GFAP–ve cells) in the rostral CC of our 12 month-old control mice. The cell densities of OL lineage cells at 12 months of age were 1.6-, and 2.0-fold higher than those seen at 2 and 6 months of age, respectively. However, by 16 months of age the OL lineage cell densities had decreased some 3.5-fold compared to the cell density seen at 12 months of age. These findings suggest the generation of new OLs may continue until at least 12 months of age in mouse CNS white matter, with an age-related loss of OLs beginning sometime prior to 16 months of age. To our knowledge, no one has assessed OL cell numbers past 16 months of age.

We also found that *Nkx2.2* expression showed an age-related increase, whereas *Olig2* expression showed an

age-related decrease, in control mice. *Olig2* is expressed by cells at all stages of the OL lineage and when localized to the nucleus in cells of this lineage it functions as a transcriptional activator, promoting the differentiation and maturation of OLs (Nicolay et al. 2007). *Nkx2.2*, on the other hand, is believed to function as a transcriptional repressor in cells of the OL lineage, in particular in repressing genes associated with differentiation and maturation such as those for proteins associated with the formation of a myelin sheath (Tochitani and Hayashizaki 2008; Watanabe et al. 2004; Wei et al. 2005). *Nkx2.2*'s expression is confined to progenitor cells, immature OLs, and also some mature OLs that have not yet begun to form a myelin sheath (Tochitani and Hayashizaki 2008; Watanabe et al. 2004). The *Nkx2.2* TF represses myelin gene expression (Gokhan et al. 2005; Wei et al. 2005), and down-regulation of its expression occurs as cells of the OL lineage express a myelinating phenotype (Watanabe et al. 2004). Watanabe et al. (2004) showed that expression of *Nkx2.2* is not needed for maintenance of mature OLs in the optic nerve of rats. Furthermore, expression of *Nkx2.2* is significantly down-regulated in terminally differentiated OLs (Watanabe et al. 2004) and knockdown of *Nkx2.2* by antisense RNA enhances OL differentiation (Tochitani and Hayashizaki 2008). Thus, the age-related increased expression of *Nkx2.2* in control and cuprizone-treated mice beginning at 12 months of age might be playing a significant role in impeding the differentiation of PDGF α R+ve progenitor cells along the OL pathway.

It also possible that increased expression of *Nkx2.2* may directly or indirectly contribute to the fate choice of PDGF α R+ve glial progenitor cells to differentiate into astrocytes, although to our knowledge this possibility has not been investigated. Sun et al. (2003) reported there are both cooperative and cross-repressive interactions between *Nkx2.2* and *Olig2*, with the protein–protein interactions depending on the homeodomain and the bHLH domain of each TF, respectively. Sun et al. (2003) demonstrated the physical interaction between these two TFs was not sufficient for OL development, although leaving open the possibility that their interaction may be needed for the formation of OLs. Hence, the cross-repressive interaction between these TFs might be altered during normal aging and in response to CNS demyelination in older animals. If this were the case, then this altered interaction could play a significant role in impeding the OL progenitor cell response during normal aging and in response to cuprizone in older mice, given that the expression levels of *Nkx2.2* in these mice are several-fold higher at 12 and 16 months of age compared to younger mice.

In spite of the increased numbers of cells of the OL lineage that were present in the 12-month-old control mice, there was a 3.1- and 2.1-fold decreased *MOG* and *CGT*

gene expression, respectively, compared to 2 month-old control mice. Although it remains to be determined if *Nkx2.2* directly represses expression of the *MOG* and *CGT* genes, increased expression of the transcriptional repressor *Nkx2.2* in 12 month-old control mice may be repressing myelin gene expression in these OL lineage cells and thus preventing them from assembling a myelin sheath. *Nkx2.2* has been shown to repress myelin gene expression (Gokhan et al. 2005; Wei et al. 2005) and down-regulation of its expression occurs as cells of the OL lineage express a myelinating phenotype (Watanabe et al. 2004). Ultrastructural quantitation of the numbers of myelinated axons in 12-month-old control mice should show whether the increased numbers of OLs we saw in control mice at this age are associated with significantly more myelinated axons compared to younger mice.

Our use of the cuprizone model on mice as old as 16 months of age has demonstrated the tissue of the CC retains the capacity to generate new OLs even in mice as old as 16 months of age. However, the OL lineage cells are drastically reduced in number in the rostral CC of 12- and 16-month-old cuprizone recovery mice, being 13.1- and 2.7-fold lower than cuprizone recovery mice at 2 months of age, and 19.7- and 4.0-fold lower than 6 month-old cuprizone recovery mice, respectively. This is evidence of an inefficient generation of new OLs to replace those lost as a result of the cuprizone-induced demyelination. It can be speculated that this reduction in the number of OL lineage cells in these older cuprizone-fed mice is due, at least in part, to the reduced PDGF α R+ve/GFAP–ve progenitor cell response to cuprizone-induced demyelination and to an increase in the number of PDGF α R+ve cells that have chosen the astrocyte pathway of differentiation.

Our data also reveal interesting new findings with respect to cells of the astrocyte lineage in the aging animal. Progenitor cells in CNS white matter are PDGF α R+ve and NG2+ve and generate progeny that differentiate along the astrocyte pathway in addition to the OL pathway, although differentiation of these progenitors into astrocytes in adult animals is believed to occur mainly in response to CNS injury (Cassiani-Ingoni et al. 2006; Magnus et al. 2007; Zhao et al. 2009). Several studies report an increase in numbers of PDGF α R+ve progenitor cells in response to spinal cord injury (Labombarda et al. 2009), lysophatidylcholine-induced CNS demyelination (Watanabe et al. 2004), autoimmune-induced CNS inflammation (i.e., experimental allergic encephalitis; EAE) (Cassiani-Ingoni et al. 2006), or a stab wound injury to the cerebral hemisphere (Magnus et al. 2007). Our data also show a demyelination-induced increase in PDGF α R+ve progenitor cells, which in 6–16 month-old mice was confined to progenitor cells in which there was cytoplasmic translocation of *Olig2* indicative of these cells having made a fate

choice to differentiate into astrocytes. The Olig2 translocation allows progenitor cells to differentiate into astrocytes probably by allowing the activation of astrocytic genes in response to extracellular stimuli. As shown by Setoguchi and Kondo (2004), for example, Olig2 translocation is crucial for CNTF-induced astrocyte differentiation. Furthermore, Fukuda et al. (2004) have shown that Olig2 prevents complex formation between the transcriptional activator p300 and the signal transducer and activator of transcription 3 (STAT3) TF. The STAT3-p300 complex is required for development of astrocytes and the ability of STAT3 and p300 to form a complex following cytoplasmic translocation of Olig2 may be enhanced in older animals.

A recent report (Islam et al. 2009) showed no increase in the percentage of GFAP+ve/GFP+ve cells in the external capsule of 8–10 week-old mice treated with cuprizone and our data also do not show a change in the Olig2^{Cyto}-ve/GFAP+ve mature astrocytes in the 2-month cuprizone mice. In this study, we quantified the numbers of cells at three different stages of the astrocyte cell lineage. These stages included astrocyte progenitor cells (Olig2^{Cyto}+ve/PDGFR+ve), newly formed astrocytes (Olig2^{Cyto}+ve/GFAP+ve) and mature astrocytes (Olig2^{Cyto}-ve/GFAP+ve cells). In congruence with the findings of Cassiani-Ingoni et al. (2006), who used the EAE model to induce CNS demyelination in adult mice (age not stated in their paper), we also found that astrocyte differentiation from progenitor cells constituted a significant source of reactive astrocytes, both in young adult and in older mice. The cell densities of Olig2^{Cyto}+ve/GFAP+ve newly formed astrocytes were significantly higher in cuprizone mice than in age-matched control mice at all 4 ages. In contrast, increased numbers of Olig2^{Cyto}-ve/GFAP+ve mature astrocytes were only seen in 6-month-old cuprizone recovery mice. Consistent with the astrocytic response to the cuprizone-induced demyelination involving the formation of new astrocytes, there were also significantly more Olig2^{Cyto}+ve/PDGFR+ve astrocyte progenitor cells present in the rostral CC in response to cuprizone-induced demyelination.

In conclusion, our findings provide some insight into why there is an age-related decreased efficiency of myelination and remyelination. The size of the progenitor cell pool seems to remain fairly constant at least up to 16 months of age, but beginning at 6 months of age these progenitor cells tend to choose differentiation along the astrocyte lineage as opposed to the OL lineage. Our findings implicate the TFs Nkx2.2 and Olig2 as important components of the transcriptional control network that may contribute to this age-related switch in fate choice of the PDGFR+ve progenitor cells. First, the age-related increased expression of the *Nkx2.2* gene would certainly

impede the differentiation of these progenitor cells into OLs, and therefore limit the extent of remyelination that can occur following cuprizone-induced demyelination. Second, an increase in the number of PDGFR+ve progenitor cells with cytoplasmic translocation of the Olig2 TF would facilitate their differentiation into astrocytes and the activation of astrocytic genes in response to extracellular stimuli. Hence, a first step in improving remyelination efficiency in older animals may require both a reversal of the age-related increased expression of the transcriptional repressor Nkx2.2 and preventing the cytoplasmic translocation of Olig2.

Acknowledgments This project was supported by an operating grant from the Canadian Institutes of Health Research (to AN and RD) and by a Pilot Project Grant from the Cameco Multiple Sclerosis Neuroscience Research Center (to RD and AN). We thank Dr. Collette Wheeler and Ms. Michele Moroz for their assistance and guidance in monitoring the health status of the mice. Special thanks are also due to R. Sobchishin and M. Basiri for technical assistance. We are also grateful to Drs. M. Gardinier and H. Takebayashi for providing the mouse monoclonal antibody to MOG and the rabbit polyclonal antibody to Olig2, respectively.

References

- Ando S, Tanaka Y, Toyoda Y, Kon K (2003) Turnover of myelin lipids in aging brain. *Neurochem Res* 28:5–13
- Armstrong RC, Le TQ, Frost EE, Borke RC, Vana AC (2002) Absence of fibroblast growth factor 2 promotes oligodendroglial repopulation of demyelinated white matter. *J Neurosci* 22:8574–8585
- Arnett HA, Fancy SP, Alberta JA, Zhao C, Plant SR, Kaing S, Raine CS, Rowitch DH, Franklin RJ, Stiles CD (2004) bHLH transcription factor Olig1 is required to repair demyelinated lesions in the CNS. *Science* 306:2111–2115
- Bakker DA, Ludwin SK (1987) Blood-brain barrier permeability during Cuprizone-induced demyelination. Implications for the pathogenesis of immune-mediated demyelinating diseases. *J Neurol Sci* 78:125–137
- Bartzokis G (2004a) Age-related myelin breakdown: a developmental model of cognitive decline and Alzheimer's disease. *Neurobiol Aging* 25:5–18 author reply 49–62
- Bartzokis G (2004b) Author's response to commentaries. Quadratic trajectories of brain myelin content: unifying construct for neuropsychiatric disorders. *Neurobiol Aging* 25:49–62
- Bartzokis G, Sultzer D, Lu PH, Nuechterlein KH, Mintz J, Cummings JL (2004a) Heterogeneous age-related breakdown of white matter structural integrity: implications for cortical "disconnection" in aging and Alzheimer's disease. *Neurobiol Aging* 25: 843–851
- Bartzokis G, Tishler TA, Shin IS, Lu PH, Cummings JL (2004b) Brain ferritin iron as a risk factor for age at onset in neurodegenerative diseases. *Ann N Y Acad Sci* 1012:224–236
- Benes FM (2004) A disturbance of late myelination as a trigger for Alzheimer's disease. *Neurobiol Aging* 25:41–43
- Blakemore WF, Crang AJ (1988) Extensive oligodendrocyte remyelination following injection of cultured central nervous system cells into demyelinating lesions in adult central nervous system. *Dev Neurosci* 10:1–11

- Blakemore WF, Crang AJ, Franklin RJM (1990) Transplantation of glial cell cultures into areas of demyelination in the adult CNS. *Prog Brain Res* 82:225–232
- Boyd JG, Lee J, Skihar V, Doucette R, Kawaja MD (2004) LacZ-expressing olfactory ensheathing cells do not associate with myelinated axons after implantation into the compressed spinal cord. *Proc Natl Acad Sci U S A* 101:2162–2166
- Braak H, Del Tredici K (2004) Poor and protracted myelination as a contributory factor to neurodegenerative disorders. *Neurobiol Aging* 25:19–23
- Carey EM, Freeman NM (1983) Biochemical changes in Cuprizone-induced spongiform encephalopathy. I. Changes in the activities of 2',3'-cyclic nucleotide 3'-phosphohydrolase, oligodendroglial ceramide galactosyl transferase, and the hydrolysis of the alkenyl group of alkenyl, acyl-glycerophospholipids by plasmalogenase in different regions of the brain. *Neurochem Res* 8:1029–1044
- Cassiani-Ingoni R, Coksaygan T, Xue H, Reichert-Scriver SA, Wiendl H, Rao MS, Magnus T (2006) Cytoplasmic translocation of Olig2 in adult glial progenitors marks the generation of reactive astrocytes following autoimmune inflammation. *Exp Neurol* 201:349–358
- Chari DM, Crang AJ, Blakemore WF (2003) Decline in rate of colonization of oligodendrocyte progenitor cell (OPC)-depleted tissue by adult OPCs with age. *J Neuropathol Exp Neurol* 62:908–916
- Collarini EJ, Pringle N, Mudhar H, Stevens G, Kuhn R, Monuki ES, Lemke G, Richardson WD (1991) Growth factors and transcription factors in oligodendrocyte development. *J Cell Sci Suppl* 15:117–123
- Connor JR (2004) Myelin breakdown in Alzheimer's disease: a commentary. *Neurobiol Aging* 25:45–47
- Franklin RJ, Zhao C, Sim FJ (2002) Ageing and CNS remyelination. *Neuroreport* 13:923–928
- Fukuda S, Kondo T, Takebayashi H, Taga T (2004) Negative regulatory effect of an oligodendrocyte bHLH factor OLIG2 on the astrocytic differentiation pathway. *Cell Death Differ* 11:196–202
- Gokhan S, Marin-Husstege M, Yung SY, Fontanez D, Casaccia-Bonnel P, Mehler M (2005) Combinatorial profiles of oligodendrocyte-selective classes of transcriptional regulators differentially modulate myelin basic protein gene expression. *J Neurosci* 25:8311–8321
- Hall SM (1972) The effect of injections of lysophosphatidyl choline into white matter of the adult mouse spinal cord. *J Cell Sci* 10:535–546
- Hao Z, Yeung J, Wolf L, Doucette R, Nazarali A (1999) Differential expression of Hoxa-2 protein along the dorsal-ventral axis of the developing and adult mouse spinal cord. *Dev Dyn* 216:201–217
- Herndon RM, Price DL, Weiner LP (1977) Regeneration of oligodendroglia during recovery from demyelinating disease. *Science* 195:693–694
- Hinks GL, Franklin RJ (2000) Delayed changes in growth factor gene expression during slow remyelination in the CNS of aged rats. *Mol Cell Neurosci* 16:542–556
- Hiremath MM, Saito Y, Knapp GW, Ting JP, Suzuki K, Matsushima GK (1998) Microglial/macrophage accumulation during cuprizone-induced demyelination in C57BL/6 mice. *J Neuroimmunol* 92:38–49
- Islam MS, Tatsumi K, Okuda H, Shiosaka S, Wanaka A (2009) Olig2-expressing progenitor cells preferentially differentiate into oligodendrocytes in cuprizone-induced demyelinated lesions. *Neurochem Internat* 54:192–198
- Jurevics H, Largent C, Hostettler J, Sammond DW, Matsushima GK, Kleindienst A, Toews AD, Morell P (2002) Alterations in metabolism and gene expression in brain regions during cuprizone-induced demyelination and remyelination. *J Neurochem* 82:126–136
- Knobler RL, Stempak JG, Laurencin M (1974) Oligodendroglial ensheathment of axons during myelination in the developing rat central nervous system. A serial section electron microscopical study. *J Ultrastruct Res* 49:34–49
- Komoly S, Hudson LD, Webster HD, Bondy CA (1992) Insulin-like growth factor I gene expression is induced in astrocytes during experimental demyelination. *Proc Natl Acad Sci USA* 89:1894–1898
- Kondo A, Nakano T, Suzuki K (1987) Blood-brain barrier permeability to horseradish peroxidase in twitcher and cuprizone-intoxicated mice. *Brain Res* 425:186–190
- Lang W, Rodriguez M, Lennon VA, Lampert PW (1984) Demyelination and remyelination in murine viral encephalomyelitis. *Ann N Y Acad Sci* 436:98–102
- Labombarda F, González SL, Lima A, Roig P, Guennoun R, Schumacher M, de Nicola AF (2009) Effects of progesterone on oligodendrocyte progenitors, oligodendrocyte transcription factors, and myelin proteins following spinal cord injury. *Glia* 57:884–897
- Ludwin SK (1978) Central nervous system demyelination and remyelination in the mouse: an ultrastructural study of cuprizone toxicity. *Lab Invest* 39:597–612
- Ludwin SK (1979) An autoradiographic study of cellular proliferation in remyelination of the central nervous system. *Am J Pathol* 95:683–696
- Ludwin SK (1980) Chronic demyelination inhibits remyelination in the central nervous system. An analysis of contributing factors. *Lab Invest* 43:382–387
- Ludwin SK, Sternberger NH (1984) An immunohistochemical study of myelin proteins during remyelination in the central nervous system. *Acta Neuropathol (Berl)* 63:240–248
- Lyman WD, Brosnan CF, Raine CS (1985) Chronic-relapsing experimental autoimmune encephalomyelitis. Myelin basic protein induces suppression of blastogenesis during remissions but not during exacerbations. *J Neuroimmunol* 7:345–353
- Magnus T, Coksaygan T, Korn T, Xue H, Arumugam TV, Mughal MR, Eckley DM, Tang SC, DeTolla L, Rao MS, Cassiani-Ingoni R, Mattson MP (2007) Evidence that nucleocytoplasmic Olig2 translocation mediates brain-injury-induced differentiation of glial precursors to astrocytes. *J Neurosci Res* 85:2126–2137
- Mason JL, Xuan S, Dragatsis I, Efstratiadis A, Goldman JE (2003) Insulin-like growth factor (IGF) signaling through type 1 IGF receptor plays an important role in remyelination. *J Neurosci* 23:7710–7718
- Matsushima GK, Morell P (2001) The neurotoxicant, cuprizone, as a model to study demyelination and remyelination in the central nervous system. *Brain Pathol* 11:107–116
- Morell P, Barrett CV, Mason JL, Toews AD, Hostettler JD, Knapp GW, Matsushima GK (1998) Gene expression in brain during cuprizone-induced demyelination and remyelination. *Mol Cell Neurosci* 12:220–227
- Nicolay D, Doucette R, Nazarali A (2007) Transcriptional control of oligodendrogenesis. *Glia* 55:1287–1299
- Noble M (2004) The possible role of myelin destruction as a precipitating event in Alzheimer's disease. *Neurobiol Aging* 25:25–31
- Peters A (2002a) Structural changes that occur during normal aging of primate cerebral hemispheres. *Neurosci Biobehav Rev* 26:733–741
- Peters A (2002b) The effects of normal aging on myelin and nerve fibers: a review. *J Neurocytol* 31:581–593
- Peters A, Sethares C (2002) Aging and the myelinated fibers in prefrontal cortex and corpus callosum of the monkey. *J Comp Neurol* 442:277–291

- Rist JM, Franklin RJ (2008) Taking ageing into account in remyelination-based therapies for multiple sclerosis. *J Neurol Sci* 274:64–67
- Rivers LM, Young KM, Rizzi M, Jamen F, Psachoulia K, Wade A, Kessaris N, Richardson WD (2008) PDGFRA/NG2 glia generate myelinating oligodendrocytes and piriform projection neurons in adult mice. *Nature Neurosci* 11:1392–1401
- Sandell JH, Peters A (2002) Effects of age on the glial cells in the rhesus monkey optic nerve. *J Comp Neurol* 445:13–28
- Setoguchi T, Kondo T (2004) Nuclear export of OLIG2 in neural stem cells is essential for ciliary neurotrophic factor-induced astrocyte differentiation. *J Cell Biol* 166:963–968
- Shen S, Sandoval J, Swiss VA, Li J, Dupree J, Franklin RJ, Casaccia-Bonnel P (2008) Age-dependent epigenetic control of differentiation inhibitors is critical for remyelination efficiency. *Nature Neurosci* 11:1024–1034
- Sim FJ, Zhao C, Penderis J, Franklin RJ (2002) The age-related decrease in CNS remyelination efficiency is attributable to an impairment of both oligodendrocyte progenitor recruitment and differentiation. *J Neurosci* 22:2451–2459
- Sloane JA, Hinman JD, Lubonia M, Hollander W, Abraham CR (2003) Age-dependent myelin degeneration and proteolysis of oligodendrocyte proteins is associated with the activation of calpain-1 in the rhesus monkey. *J Neurochem* 84:157–168
- Stidworthy MF, Genoud S, Suter U, Mantei N, Franklin RJ (2003) Quantifying the early stages of remyelination following cuprizone-induced demyelination. *Brain Pathol* 13:329–339
- Sun T, Dong H, Wu L, Kane M, Rowitch DH, Stiles CD (2003) Cross-repressive interaction of the Olig2 and Nkx2.2 transcription factors in developing neural tube associated with formation of a specific physical complex. *J Neurosci* 23:9547–9556
- Tochitani S, Hayashizaki Y (2008) Nkx2.2 antisense RNA overexpression enhanced oligodendrocytic differentiation. *Biochem Biophys Res Commun* 372:691–696
- Watanabe M, Hadzic T, Nishiyama A (2004) Transient upregulation of Nkx2.2 expression in oligodendrocyte lineage cells during remyelination. *Glia* 46:311–322
- Wegner M (2000a) Transcriptional control in myelinating glia: flavors and spices. *Glia* 31:1–14
- Wegner M (2000b) Transcriptional control in myelinating glia: the basic recipe. *Glia* 29:118–123
- Wegner M (2001) Expression of transcription factors during oligodendroglial development. *Microsc Res Tech* 52:746–752
- Wei Q, Miskimins WK, Miskimins R (2005) Stage-specific expression of myelin basic protein in oligodendrocytes involves Nkx2.2-mediated repression that is relieved by the Sp1 transcription factor. *J Biol Chem* 280:16284–16294
- Yajima K, Suzuki K (1979) Ultrastructural changes of oligodendroglia and myelin sheaths induced by ethidium bromide. *Neuropathol Appl Neurobiol* 5:49–62
- Zeller NK, Behar TN, Dubois-Dalcq ME, Lazzarini RA (1985) The timely expression of myelin basic protein gene in cultured rat brain oligodendrocytes is independent of continuous neuronal influences. *J Neurosci* 5:2955–2962
- Zhao J-W, Raha-Chowdhury R, Fawcett JW, Watts C (2009) Astrocytes and oligodendrocytes can be generated from NG2 + progenitors after acute brain injury: intracellular localization of oligodendrocyte transcription factor 2 is associated with their fate choice. *Eur J Neurosci* 29:1853–1869